Journal of Neuroinflammation

RESEARCH

Open Access

Enhanced phagocytosis associated with multinucleated microglia via Pyk2 inhibition in an acute β-amyloid infusion model

Ji-Won Lee[1*], Kaito Mizuno[1,2], Haruhisa Watanabe[3,6], In-Hee Lee[4], Takuya Tsumita[5], Kyoko Hida[5], Yasutaka Yawaka[2], Yoshimasa Kitagawa[6], Akira Hasebe[1], Tadahiro Iimura[3] and Sek Won Kong[4,7]

Abstract

Multinucleated microglia have been observed in contexts associated with infection, inflammation, and aging. Though commonly linked to pathological conditions, the larger cell size of multinucleated microglia might enhance their phagocytic functions, potentially aiding in the clearance of brain debris and suggesting a reassessment of their pathological significance. To assess the phagocytic capacity of multinucleated microglia and its implications for brain debris clearance, we induced their formation by inhibiting Pyk2 activity using the pharmacological inhibitor PF-431396, which triggers cytokinesis regression. Multinucleated microglia demonstrate enhanced phagocytic function, as evidenced by their increased capacity to engulf β-amyloid (Aβ) oligomers. Concurrently, the phosphorylation of Pyk2, induced by Aβ peptide, was diminished upon treatment with a Pyk2 inhibitor (Pyk2-Inh, PF-431396). Furthermore, the increased expression of Lamp1, a lysosomal marker, with Pyk2-inh treatment, suggests an enhancement in proteolytic activity. In vivo, we generated an acute Alzheimer's disease (AD) model by infusing Aβ into the brains of Iba-1 EGFP transgenic (Tg) mice. The administration of the Pyk2-Inh led to an increased migration of microglia toward amyloid deposits in the brains of Iba-1 EGFP Tg mice, accompanied by morphological activation, suggesting a heightened affinity for Aβ. In human microglia, lipopolysaccharide (LPS)-induced inflammatory responses showed that inhibition of Pyk2 signaling significantly reduced the transcription and protein expression of pro-inflammatory markers. These results suggest that Pyk2 inhibition can modulate microglial functions, potentially reducing neuroinflammation and aiding in the clearance of neurodegenerative disease markers. This highlights Pyk2 as a promising target for therapeutic intervention in neurodegenerative diseases.

Keywords Protein Tyrosine Kinase 2B, Microglia, Multinucleation, Phagocytosis, β-amyloid, Alzheimer's disease

*Correspondence:
Ji-Won Lee
jwlee@den.hokudai.ac.jp
[1] Microbiology, Department of Oral Pathobiological Science, Faculty and Graduate School of Dental Medicine, Hokkaido University, Kita13 Nishi7, Kita-Ku, Sapporo 060-8586, Japan
[2] Dentistry for Children and Disabled Persons, Department of Oral Functional Science, Faculty of Dental Medicine, Hokkaido University, Kita13 Nishi7, Kita-Ku, Sapporo 060-8586, Japan
[3] Department of Pharmacology, Faculty and Graduate School of Dental Medicine, Hokkaido University, Kita13 Nishi7, Kita-Ku, Sapporo 060-8586, Japan
[4] Computational Health and Informatics Program, Boston Children's Hospital, Boston, MA 02215, USA
[5] Department of Vascular Biology and Molecular Pathology, Faculty and Graduate School of Dental Medicine, Hokkaido University, Kita13 Nishi7, Kita-Ku, Sapporo 060-8586, Japan
[6] Oral Diagnosis and Medicine, Department of Oral Pathobiological Science, Faculty of Dental Medicine, Hokkaido University, Kita13 Nishi7, Kita-Ku, Sapporo 060-8586, Japan
[7] Department of Pediatrics, Harvard Medical School, Boston, MA 02115, USA

Background

Alzheimer's disease (AD) is a complex neurodegenerative disorder characterized by progressive cognitive decline, memory loss and impaired executive function [1]. Representative hallmark of AD is the accumulation of β-amyloid (Aβ) plaque in the brain [2]. Aβ peptides are derived from the cleavage of amyloid precursor protein (APP) by enzymes such β-secretase and ɣ-secretase [3]. These Aβ peptides aggregate to form insoluble plaques, which are neurotoxic and disrupt neuronal function. As such, the genes involved in the production and process APP, including *APP, PSEN1, PSEN2* (components of the ɣ-secretase complex), and *BACE1* (β-secretase), have been consistently reported as genetic risk factors for familial AD [4]. However, small molecules and biologics targeting β-secretase or ɣ-secretase complex have not been successful in reduced Aβ production [5–10]. Therefore, alternative therapeutic strategies to effectively prevent Aβ accumulation are urgently needed to prevent and delay the progression of AD.

Phagocytosis is the process by which immune cells engulf and digest foreign particles, pathogens, and cellular debris. In the brain, microglia play a central role in phagocytosing Aβ plaques [11]. Enhancing the clearance of Aβ plaque through microglial phagocytosis represents a potential therapeutic strategy to mitigate Aβ-induced neurotoxicity and slow disease progression in AD [12]. Microglia phagocytosis of Aβ can also modulate neuroinflammatory responses [13]. Efficient clearance of Aβ by microglia may dampen neuroinflammation by reducing the accumulation of Aβ plaques and the release of proinflammatory cytokines, thereby attenuating neuronal damage and preserving cognitive function.

Microglia, the tissue-resident macrophages derived from yolk-sac myeloid progenitors, migrate to the central nervous system (CNS) during fetal brain development, playing a crucial role in brain development, homeostasis and responding to pathological conditions [14]. The activation and functions of microglia are closely linked to various neurodegenerative diseases, including Alzheimer's disease (AD) [15–17], Parkinson's disease (PD) [18, 19], and multiple sclerosis (MS) [20–22]. As innate immune cells of the CNS, once activated, microglia participate in the clearance of misfolded proteins, debris, and pathogens, thereby mitigating neuroinflammation and preserving neuronal integrity [23, 24]. The inefficient phagocytic activity of microglia with aging may lead to the formation of Aβ plaques, neuronal dystrophy characterized by tau accumulation, and neuroinflammation, which collectively represent the core pathologies of AD [25, 26]. Microglial activation and phagocytosis are intricately linked to rapid cytoskeletal remodeling and focal adhesion, which encompasses membrane ruffling and extension [27]. The cytoskeleton facilitates the bringing together of surface receptors and their substrates to regulate signal transduction, thereby transitioning microglia from an inactive state to an active state [28]. Hence, the capability for rapid morphological change in response to diverse stresses is essential for microglia phagocytosis.

Genetic studies of late-onset AD (LOAD) have identified various risk factors [29, 30]. The Protein Tyrosine Kinase 2 Beta (*PTK2B)* gene, which encodes protein tyrosine kinase (Pyk2), a non-receptor tyrosine kinase and a member of the focal adhesion kinase (FAK) family, has been identified as a genetic risk factor in genome-wide association studies (GWAS) for LOAD [29]. Indeed, Pyk2 is expressed in diverse brain cells of AD patients [30–35]. Unlike FAK, which is ubiquitously expressed across various cell types, Pyk2 expression is predominantly found in cells of the CNS and hematopoietic cells [36, 37]. Pyk2 is activated by various extracellular signals including cytokines, intracellular Ca^{2+} concentration, and integrin-mediated cell adhesion [38] and has diverse physiological and pathological roles in cell adhesion [39], migration [40], inflammatory responses [41, 42], tumor invasiveness [43] and neuronal plasticity [44]. Although *PTK2B* is recognized for its expression in neuronal cells [45, 46], recent studies have highlighted its significant role in microglia [47]. Thus, understanding the functional role of Pyk2 in microglia and its impact on AD progression is crucial for uncovering novel pathophysiological mechanisms underlying AD.

In the current study, we found that the pharmacological inhibitor, PF-431396, targeting Pyk2, leads to microglial multinucleation, irrespective of infection or inflammation responses. These multinucleated microglia exhibit enhanced phagocytosis and lysosomal activity compared to their mononuclear counterparts. To this end, we established an acute AD mouse model by directly infusing Aβ into the intracerebroventricular (ICV) region of brain using brain infusion kit in Iba-1 EGFP Tg mice. This approach enables efficient observation of microglial response to Aβ, circumventing the several months typically required for genetic AD mouse models. Administration of PF-431396 not only enhanced microglial activity but also improved phagocytosis, aiding in the removal of Aβ oligomers from the brains of Iba-1 EGFP Tg mice. Our findings indicate that pharmacological inhibition of Pyk2 signaling could offer potential in treating or delaying the onset and progression of neurodegenerative disorders such as AD, through the modulation of microglial phagolysomal activity.

Materials and methods

Preparation of Pyk2-Inh and β-amyloid

Pyk2 inhibitor (Pyk2-Inh, PF-431396, CAS no. 717906-29-1) was purchased from TOCRIS Biosciences/Biotechne (Minneapolis, MN) and dissolved in dimethyl sulfoxide (DMSO) (Sigma, MO), then diluted to corresponding concentrations. All the control group was treated with an equivalent percentage of DMSO. The final concentration of DMSO did not exceed 0.01%. Murine recombinant CSF1 was obtained from PeproTech (Cat. no. AF-315-02, Japan). Lyophilized synthetic unlabeled β-amyloid peptide (1–42, Abcam Cat. no. ab120959) were dissolved in 1% NH_4OH (Anaspec, Cat. no. As-61322) at 1 mg/mL and vortexed for 30 s according to the manufacturer's protocol [48, 49]. The peptides were then lyophilized and stored at − 80 ℃ until use. For experiments, the peptides were reconstituted in 10 mM sodium phosphate buffer (pH 7.4) at a concentration of 1 mg/mL. β-amyloid (1–42) HiLyte™ Fluor555-labeled peptide (Anaspec Inc., Cat. no. AS-60480-01) was reconstituted in a buffer containing 50 mM Tris (pH 7.4) and 0.1% NH_4OH and stored at − 80 ℃ until use according to the manufacturer's protocol. The peptide was diluted with a PBS at a working concentration of 1 mg/mL. For brain injection, the Aβ peptide was diluted in artificial cerebrospinal fluid (ACSF, TOCRIS, Cat. No. 3525), incubated at 37 ℃ for 10 min, and then placed on ice before use [50].

Animals

Iba-1 EGFP Tg mice were obtained from RIKEN BRC (Japan). Mice were housed under controlled lighting conditions (daily light, 07:00–21:00) and were maintained under specific pathogen-free conditions. A total of 6 mice were randomly divided into two groups (n = 3 per group) with a weight deviation of less than 5% and compared pharmacological phenotypes of Pyk2-Inh in 7-week-old Iba-1 EGFP Tg mice (littermates, female).

Cell cultures

The mouse microglia cell line MG6 (Riken BRC, Japan) was cultured in Dulbecco's Modified Eagle Medium (DMEM—high glucose, Gibco, Life Technologies Corporation, CA) supplemented with 10 μg/mL insulin, 0.1 mM 2-mercaptoethanol (2-ME, Sigma) and 10% fetal bovine serum (FBS) at 37 ℃ in a humidified atmosphere of 5% CO_2. The human microglia cell line HMC3 (ATCC, CRL-3304, VA) was cultured in Minimum Essential Medium Eagle (MEME, Sigma) supplemented with non-essential amino acid, sodium pyruvate and 10% FBS at 37 ℃ in a humidified atmosphere of 5% CO_2. The medium was changed every 3 days until harvested.

Cell proliferation assay

Cells were seeded in a 96-well plate (1×10^4 cells/well) and cultured at 37 ℃ for 24 h. Cell proliferation was determined by a 3-(4,5-dime-thylthiazol-2-yl)-2,5-diphenyltetrazolium bromide assay with Cell Count Kit-8 (Dojindo, Japan) according to the manufacturer's protocol. Measurement was carried out in absorbance at 570 nm with a microplate reader (Bio-Rad, Japan). The cell viability was standardized to the relative control as a percentage.

Quantitative RT-PCR (qPCR)

Total RNA was extracted from cells using RNAeasy® Mini kit (Qiagen, Hilden, Germany) according to the manufacturer's protocol. RNA was quantified using a spectrophotometry (DeNovix, DS-11, Japan). The template RNA was used to generate complementary DNA (cDNA) via a Reverse Transcription Kit according to the manufacturer's instructions on ice (QuantiTect®, Qiagen). Quantitative real-time RT-PCR was carried out with DNA probes PowerUp SYBR Green Master Mix (Thermo Fisher, CA). The primer sequences (Eurofins Genomics, Japan) were listed in Supplemental Table 1. To normalize the amount of RNA, the expression of *Gapdh* and *RPLP0* were chosen as the endogenous control for mouse and human, respectively. Expression of target mRNA was calculated from 2Δ Ct values.

Immunoblotting analysis

Total protein was extracted from cells using ice-cold radio immunoprecipitation assay buffer (RIPA, Abcam) containing protease and phosphatase inhibitor cocktail (Sigma) and incubated on ice for 10 min. Cell lysis was centrifuged at 12,000 rpm at 4 ℃ for 10 min and supernatants were separated by 7.5% Mini-PROTEAN TGX Gels (Bio-Rad, USA) electrophoresis and transferred to polyvinylidene fluoride membranes (PVDF, Bio-Rad). The membranes were blocked with 5% bovine serum albumin (BSA) in Tris-Buffered Saline with Tween 20 (TBST) (pH 7.6) (Takara Bio, Japan) for 30 min at room temperature with gentle shaking, followed by incubation with primary antibodies overnight at 4 ℃. The primary antibodies detected immuno-blotting were listed as follows: p-Pyk2 (Anti-rabbit, Cell Signaling Technology #3291, 1:1000), Pyk2 (Anti-rabbit, Cell Signaling Technology #3292, 1:1000), pFAK (Anti-rabbit, Cell Signaling Technology #3283, 1:1000), FAK (Anti-Rabbit, Cell Signaling Technology #3285, 1:1000), p-ERK (Anti-Rabbit, Cell Signaling Technology #4370, 1:1000), ERK (Anti-Rabbit, Cell Signaling Technology #9102, 1:1000), p-Src (Anti-rabbit,

Cell Signaling Technology #6943, 1:1000), Src (Anti-rabbit, Cell Signaling Technology #2108, 1:1000), Mannose receptor (Anti-mouse, Abcam ab64693, 1:1000), Lamp-1 (Anti-rabbit, Abcam ab24170, 1:1000), p-NF-κB (Anti-rabbit, Cell Signaling Technology #3033, 1:1000), NF-κB (Anti-rabbit, Cell Signaling Technology #8242, 1:1000), β-actin (Anti-mouse, Wako, 010-27841, 1:1000) and Tubulin (Anti-rat, Abcam ab6160, 1:1000). The membranes were washed 3 times with 1×TBST for 10 min, then added secondary antibodies (Anti-Rabbit, EnVision+System- HRP Labelled Polymer Dako, USA) or (Anti-mouse, EnVision+System-HRP Labelled Polymer, Dako, USA) for 1.5 h at room temperature with gentle shaking. The protein bands were visualized using a Clarity™ Western ECL Substrate (Bio-Rad, US) and exposed to an iBright CL1500 Imaging System (Invitrogen). Results were standardized using housekeeping protein.

Phagocytosis of *E. coli* BioParticles

Microglia treated with Pyk2-Inh for 24 h were sorted into mononucleated and multinucleated cells using a fluorescence-activated cell sorter (FACS, BD Biosciences). Briefly, MG6 cells were stained with Hoechst 33,342 for 5 min before being loaded into the FACS. Then, cells with or without Pyk2-Inh were suspended in autoMACS® Running Buffer (Myltenyi Biotec, CA). Sorting was based on the size difference between mononucleated cells (small) and multinucleated cells (large). The small cell fraction and the large cell fraction were distinguished using forward scatter-area (FSC-A) and side scatter-area (SSC-A) and then sorted by BD FACSAria™II Cell Sorter respectively. Sorted MG6 cells were seeded at a density of 5×10^3 cells/well in a plate. pHrodo Red *E. coli* BioParticles (Invitrogen), at a concentration of 10 μg/mL, were added to the MG6 cells, and the culture was incubated at 37 ℃ for 30 min to 4 h to allow phagocytosis and acidification until to reach their maximum level. At every indicated time points, fluorescence was measured using fluorescence plate reader (PerkinElmer Wallac1420 ARVO™SFL1) with excitation 560 nm and emission 585 nm wavelength. For imaging analysis, MG6 cells were seed in a μ-slide 8-well chamber (ibidi, Germany). After 30 min of exposure to BioParticles, cells were fixed with 10% formalin and subjected to immunocytochemistry. Particles were quantified by IMARIS software.

Lysosomal activity

To measure the lysosomal activity, we utilized the DQ™ Green bovine serum albumin (BSA) (Invitrogen, cat. no. D12050). The conjugated BODIPY dye (self-quenched status) produces fluorescence (dequenching status) through intracellular degradation of fluorescein derivatives by proteolysis activity. MG6 cells were seeded at 1 $\times 10^5$ cells/well in a 96-well black clear bottom plate and cultured in medium containing CSF1 (100 ng/mL). After 24 h, Pyk2 inhibitor was added at varying concentrations (0, 500, 1000 nM). Following another 24 h, DQ Green BSA was administered at a concentration of 20 μg/mL, and fluorescence was measured using fluorescence plate reader (PerkinElmer Wallac1420 ARVO™SFL1) with excitation 355 nm and emission 460 nm wavelength after 3 h.

Immunohisto – and cytochemistry analysis

MG6 cells were treated with or without Pyk2-Inh (1000 ng/mL) in the presence of Aβ at a concentration of 500 ng/mL. For immunostaining, cells were fixed with 4% paraformaldehyde in PBS for 10 min, permeabilized with 0.1% Triton X-100/PBS for 30 min, followed by blocking with 0.1% BSA (Sigma) for 30 min. Cells were stained with the indicated specific antibodies. The primary antibodies detected immuno-cytochemistry and -histochemistry were listed as follows: Iba-1 (Anti-Rabbit, Wako, 019-19741, 1:200), Tubulin (Anti-rat, Abcam ab6160, 1:100), Pericentrin (Anti-rabbit, Abcam, ab4448, 1:100) and IntegrinαV (Anti-mouse, Abcam, ab16821, 1:100). To quench the fixation agent and eliminate any free aldehyde groups that could non-specifically bind antibodies, sections or cells were treated with 0.1 M Tris buffer. Immunofluorescence images were captured using a laser confocal scanning microscope (A1-ECLIPSE Ti2-E, Nikon, Japan) equipped with an oil immersion objective lens, PLAN APO λD 60X (NA = 1.42). Prior to performing live-cell imaging, cells cultured in the chamber slide were incubated with Hoechst 33,342 (ThermoFisher Scientific) for 10 min. Then, the chamber slide was placed on an onstage incubator equipped with A1-ECLIPSE Ti2-E. Time-lapse sequence images of microglia were acquired every 10 s. All images were processed for quantification using NIS-Elements (Nikon), IMARIS (Bitplane, Zurich, Switzerland) and ImageJ software programs.

Brain infusion and drug delivery using osmotic pump in vivo

The mice were anesthetized using a combination of ketamine and isoflurane. Initially, ketamine was administered via intraperitoneal injection, followed by induction of anesthesia with isoflurane inhalation. Throughout the surgical procedure, anesthesia was maintained with continuous administration of isoflurane. A hall for microneedle injection was created in the skull using a dental drill at coordinated 0.5 mm in the anteroposterior axis, ± 1 mm in the mediolateral axis and − 2.5 mm in the dorsoventral axis from bregma [51]. Subsequently, a microneedle (28 gauge) from the brain infusion kit (Alzet Osmotic Pump, CA) was inserted into the intracerebroventricular (ICV)

space of the mouse. The osmotic pump (model 1003D, delivery rate 1.026 µL/hour, duration for 3 days) containing Pyk2-Inh or β-amyloid solution (10 µg/100 µL), was assembled with the brain infusion kit, and then implanted underneath the skin on the mouse's back. Each reagent was infused into the osmotic pump to maintain a constant rate of infusion for 3 days. Both Pyk2-Inh and β-amyloid were diluted in fresh sterile artificial cerebrospinal fluid (ACSF composition: Na 150 mM; K 3.0 mM; Ca 1.4 mM; Mg 0.8 mM; P 1.0 mM; Ci 155 mM) at 37 ℃ for 10 min before placing on ice. Vehicle group was injected with only ACSF instead of Pyk2-Inh to match the conditions of the experimental treatments. For the first 3 days, Pyk2-Inh or vehicle was injected into ICV region through an osmotic pump. This was followed by β-amyloid injection into each groups, with brain analysis performed 3 days later (Fig. 5A). All evaluations for microglial (surface, volume, length, phagocytosis etc.), neuronal cell (neu-N+analysis) parameters were conducted on the final day of the experiments.

Acute brain slice and imaging preparation

Mice were decapitated under anesthesia. The brains were dissociated on cold ACSF and sliced using a brain slicer at 1 mm thickness [52, 53]. Then, brain slices were fixed with 4% paraformaldehyde solution for 1 h. For further immunohistochemistry analysis, brain slices were incubated in the RapiClear 1.52 solution as per the manufacturer's instructions (SunJin Lab's, Hsinchu City, Taiwan). The primary antibody of NeuN (Anti-mouse, Abcam, ab104224, 1:100) was used for immunohistochemistry. All slices were analyzed using a laser confocal scanning microscope (A1-ECLIPSE Ti2-E, Nikon, Japan) at X60 magnification.

Measurement of IL-6 by ELISA

The human IL-6 expression levels in the culture supernatant were analyzed using the human IL-6 ELISA MAX™ Deluxe set (Biolegend, CA) according to the manufacturer's instructions. Cells were seeded at a density of 1×10^4 cells/well in a 96-well plate and cultured for 24 h. Cells were pretreated with Pyk2 inhibitor as indicated concentration for 3 h and the procedure was followed by exposure to 1 µg/mL LPS (*Escherichia coli* serotype 0111:B4, Sigma) for 24 h. The supernatant was collected after centrifugation was stored at − 20 ℃ until further use.

Statistical analysis

Results were shown as mean ± SEM. Statistical significance was determined using GraphPad Prism 9 (GraphPad Software Inc., CA) software program. The data were analyzed using Student's *t test* for simple comparisons or One-way ANOVA for multiple comparisons. *P*-value of < 0.05 represented statistical significance. NS indicates that the result was not significant.

Results

Pharmacological inhibition of Pyk2 activity leads to the multinucleation of microglia

Pyk2$^{-/-}$ mice are viable and fertile, without disability in development or behavior [54]. However, macrophages isolated from *Pyk2*$^{-/-}$ mice were impaired to migrate in response to chemokine stimulation [54]. To investigate the morphological and functional effects of Pyk2 inhibition in microglia, MG6 cells were treated with various doses (range 100 to 1000 nM) of PF-431396 (hereafter referred to as Pyk2-Inh). Morphological analysis revealed the presence of multinucleated microglia in MG6 cells treated with 1000 nM Pyk2-Inh for 24 h whereas such cells were absent in the vehicle-treated group (Fig. 1A). Multinucleated microglia treated with Pyk2-Inh also showed intracellular expression of ionized calcium-binding adaptor molecule 1 (Iba-1, green), a characteristic marker of activated microglia, as well as Tubulin (magenta), a constituent of the cellular cytoskeleton (Fig. 1A). Significantly, quantitative morphometric analysis showed that more than 30% of microglia were multinucleated when treated with 1000 nM Pyk2-Inh for 24 h (Fig. 1B and C).

Next, we evaluated the effects of Pyk2 inhibition on MG6 cell proliferation using the Cell Counting Kit-8 (CCK-8). Colony-Stimulating Factor 1 (CSF1) is known to regulate the survival, activation and proliferation of microglia [55], which are the resident immune cells of the CNS. By treating microglia with CSF1 showed to significantly enhance the cell proliferation, doubling compared to untreated conditions (Fig. 1D). Our findings revealed a dose-dependent response to Pyk2-Inh treatment for 24 h. Specifically, MG6 cell proliferation remained unchanged at concentrations up to 100 nM Pyk2-Inh (97.46 ± 3.11%) compared to the CSF1-treated control group (100 ± 1.98%). However, a significant decrease in proliferation was noted in cells treated with 500 nM (96.60 ± 2.24%) and 1000 nM concentrations (96.50 ± 1.75%) (Fig. 1D). Microglial survival relies on the CSF1 and CSF1 Receptor (CSF1R) signaling pathway, which includes Pyk2, Fak, Src, and Erk (Fig. 1E and F). Phosphorylated Pyk2 levels increased in response to CSF1 treatment for 10 min but were significantly reduced following Pyk2-Inh treatment, which indicates Pyk2 activity was effectively inhibited, with the p-Pyk2/Pyk2 ratio decreasing from 1.35 ± 0.08 to 0.26 ± 0.11-fold. Similarly, Pyk2-Inh treatment led to decreased phosphorylation of Fak and Src, with fold changes of 1.48 ± 0.17 to 0.22 ± 0.06-fold and 1.38 ± 0.07 to 0.24 ± 0.11-fold, respectively, compared

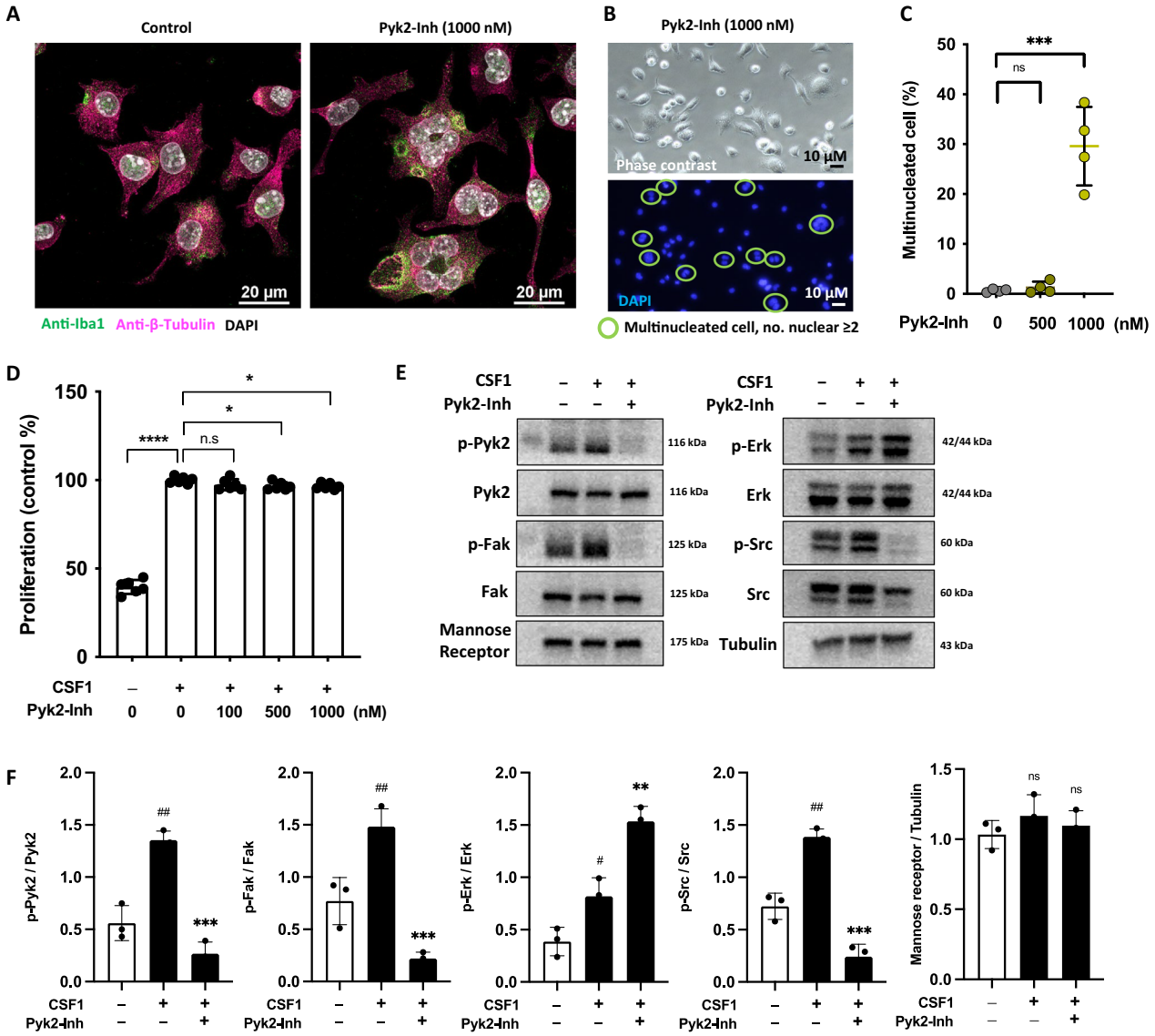

Fig. 1 Inhibition of Pyk2 signaling induces multinucleation formation in microglia. **A** Morphological changes between mononuclear and multinucleated microglia. Immunocytochemistry of MG6 cells stained with anti-Iba1 (green) and anti-β-tubulin (magenta). Nuclear DNA was labeled with DAPI (white). Scale bar is 20 μm. **B** Cells were treated with Pyk2-Inh for 24 h. Phase contrast images (upper panel) and DAPI stained images (lower panel) were shown. Circles are indicated as multinucleated cells. **C** The quantification of the number of multinucleated cells/well (control: n = 4, Pyk2-Inh-500 nM: n = 4, Pyk2-Inh-1000 nM). **D** Cell proliferation was assessed by CCK-8. MG6 cells were treated with 100 μg/mL CSF1 and indicated concentration of Pyk2-Inh (n = 6 per group, One-way ANOVA, $p < 0.05$). **E** Representatives immunoblot images. The ratio of p-Pyk2/Pyk2, pFAK/FAK, p-ERK/ERK, p-Src/Src and Mannose receptor/Tubulin were described under the blot. Pyk2-Inh was administered as a pre-treatment two hours before stimulation with CSF1 (100 μg/mL). **F** Image quantification and analysis were performed. The same experiments were repeated three times. All full-length uncropped original western blots are included in a Sup. Fig. 4. Values are mean ± SD. #: negative control (without CSF1) vs control (with CSF1), ##: $p < 0.01$; *: control (with CSF1) vs Pyk2-Inh (with CSF1), *: $p < 0.05$; **: $p < 0.01$; ***: p-value < 0.001; ****: p-value < 0.0001

to untreated conditions. Meanwhile, the expression of p-Erk signaling notably increased upon treatment with the Pyk2-Inh, with the p-Erk/Erk ratio increasing from 0.82 ± 0.17 to 1.54 ± 0.14-fold. The mannose receptor, known to be expressed in microglia, could participate in multiple physiologic and pathologic conditions [56]. However, treatment with Pyk2-Inh did not elicit any significant changes.

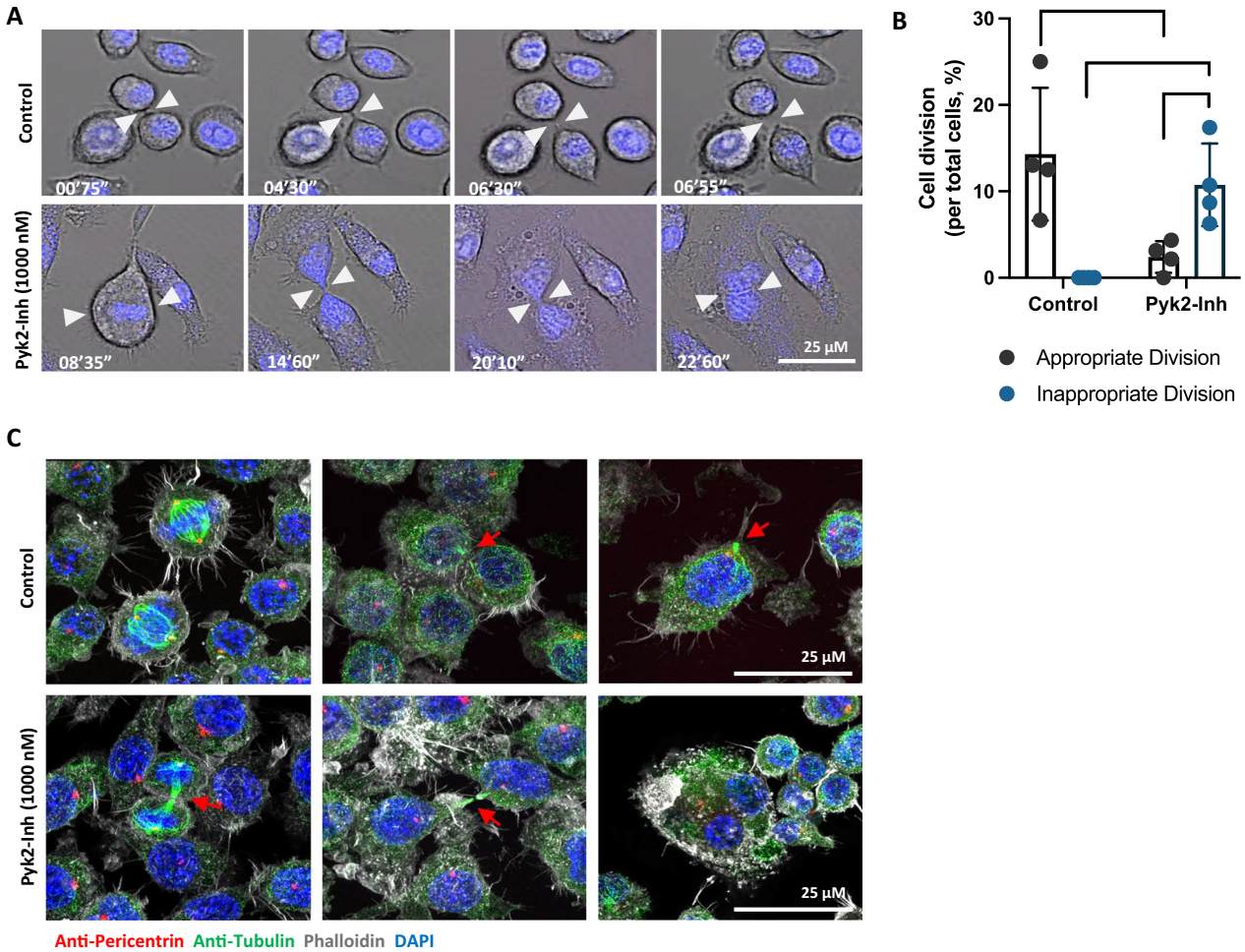

Fig. 2 Multinucleated cells are generated from abscission failure in cytokinesis, not cell fusion. **A** Dynamics of cell division by time-lapse video microscopy. The phase contrast images of the microglia's mitosis at different times. Nuclei were observed with Hoechst 33,342 staining. Arrowheads indicate representative images from anaphase to cytokinesis (control: n = 4, Pyk2-Inh: n = 4). **B** Cell division was quantified, categorizing it as either appropriate or inappropriate, in both control (n = 4) and Pyk2-Inh treated groups (n = 4). **C** Fluorescence images of microglia cells showing the stages of cell division. Immunocytochemistry of MG6 cells stained with anti-Pericentrin (red), anti-β-tubulin (green) and phalloidin (white). Nuclear DNA was labeled with DAPI (blue). Independent experiments were performed at least three times

Abnormal abscission during cytokinesis, rather than cell fusion, leads to multinucleation in microglia treated with Pyk2-Inh

To better understand the process of multinucleation, live cell imaging was conducted after treatment with Pyk2-Inh (Fig. 2A). In the control group, microglial cell membranes constricted successfully during telophase, with the separated chromosomes (stained blue with Hoechst 33,342). Following cell division, these cells naturally divided into two distinct daughter cells (Fig. 2A upper panel and Sup. Movie 1). In contrast, microglia treated with 1000 nM Pyk2-Inh showed divided chromosomes aligning at the centromere, with round shape of mature nuclei forming (confirmed with Hoechst 33,342 staining). Despite cell membrane contraction, these cells ultimately regressed to a single entity while retaining two nuclei over time (Fig. 2A lower panel and Sup. Movie 2). In Fig. 2B, the abnormalities in cell division were quantified for the control group (n = 4) and the Pyk2-Inh-treated group (n = 4). The percentage of appropriate and inappropriate divisions was compared to the total number of cells in each treatment group. As a result, the control group showed appropriate division (14.3 ± 7.69%) and inappropriate division (0%), but the Pyk2-Inh-treated group showed appropriate division (2.42 ± 1.84%) and inappropriate division (10.76 ± 4.78%). Statistically, within the Pyk2-Inh-treated group, the comparison between appropriate and inappropriate division showed a significant increase in inappropriate divisions. Additionally, compared to the control group, the Pyk2-Inh-treated

group showed a significant decrease in appropriate divisions and a significant increase in inappropriate divisions. This demonstrates that Pyk2 inhibitor treatment induces multinucleation due to abnormalities in division.

To investigate the cell division process more closely, immunofluorescence staining was utilized to highlight actin, microtubules, and centrosomes (Fig. 2C). This approach revealed that in multinucleated microglia treated with Pyk2-Inh, microtubule bundle (shown in green, indicated by red arrow) continued to persist between two cells after cell division and eventually to reaggregate into a single entity (Fig. 2C lower panels). The cleavage furrow in this process may be functionally defected, which is a crucial player in constricting the cell membrane and separating it into two daughter cells [57]. Since centrosomes are pivotal during cell division [58, 59], we confirmed whether appropriate cell division occurs by constructing an appropriate division apparatus around each nucleus in multinucleated microglia by Pyk2-Inh. There were no observed defects in centrosome formation, as indicated by staining with anti-Pericentrin (shown in red). These results indicate that multinucleation induced by Pyk2 inhibition results in improper cell division due to abscission failure attributed to cytoskeletal abnormalities, rather than cell fusion.

Multinucleated microglia enhance phagocytotic function compared to mononucleated microglia

To assess functional differences in phagocytic activity between multinucleated and mononuclear microglia after Pyk2 inhibition, phagocytic function was quantified. Both mononuclear and multinucleated microglia, isolated by FAC sorting following Pyk2-Inh treatment (Sup. Figure 1), were then exposed to pHrodo BioParticles-Red, a fluorogenic phagocytic substrate derived from *E. coli*. Microglia treated with Pyk2-Inh and untreated (control) mononuclear microglia efficiently engulfed the BioParticles (Fig. 3A upper panel). To further examine the differences in phagocytosis between mononucleated and multinucleated microglia, cells treated with Pyk2-Inh underwent confocal microscopy analysis to produce three-dimensional images of the phagocytosed BioParticles (Red). For imaging analysis, the entire cell cytoskeletal was stained with phalloidin (green), and the nucleus was stained with DAPI (white) to distinguish between mononuclear and multinuclear cell (Fig. 3A upper panels). Subsequently, these images were quantified using IMARIS imaging software (Fig. 3A lower panel and B). We observed no difference in phagocytosis between control and Pyk2-Inh treated mononucleated microglia; however, Pyk2-Inh treated multinucleated microglia exhibited a significant increase in phagocytosis (Fig. 3B). The average number of BioParticles phagocytosed per cell was counted as 86.46 ± 38.52 in the naïve control group (n = 4 per group), 106.7 ± 69.63 in the Pyk2-Inh-mono group (n = 4 per group), and 199.05 ± 98.91 in the Pyk2-Inh-multi group (n = 4 per group). Each independent experiment was conducted at three times to analyze the number of cells in Fig. 3B.

Next, we examined how phagocytosis evolved over time following Pyk2-Inh treatment. Cells separated through FAC sorting were cultured, and exposed to pHrodo BioParticles, and the fluorescence intensity was recorded at designated time intervals (Fig. 3C and D). Notably, in multinucleated cells, a marked enhancement in fluorescence, indicative of increased phagocytic activity, was observed beginning 3 h after pHrodo BioParticles treatment (Fig. 3D). Compared to the control group (phagocytosis average 100%), the phagocytosis of Pyk2-Inh treated multinucleated microglia increased more than twofold to 226.21% at 4 h (Fig. 3E). In contrast, the Pyk2-Inh treated mononucleated microglia group showed a decreased, averaging 81.77%, although this was not statistically significant. Additionally, considering that multinucleated cells may either be short-lived or revert to a mononuclear state via cytokinesis, we investigated the survival differences between multinucleated and mononucleated microglia. The survival rates of each cell type, post-sorting, were monitored over 24 h using the CCK-8 (Fig. 3F). Multinucleated cells by Pyk2-Inh demonstrated a slight increase in cell proliferation compared

(See figure on next page.)

Fig. 3 Comparison of phagocytotic function in multinucleated versus mononucleated microglia. **A** Immunofluorescence imaging depicting phagocytosis of pHrodo Red *E.coli* BioParticles by mononuclear and multinucleated MG6 cells after exposure to Pyk2-Inh. Cells were treated with pHrodo Red *E. coli* BioParticles for 1 h and fixed with paraformaldehyde. Actin cytoskeleton and nuclear DNA were stained with phalloidin (green) and DAPI (white), respectively. Engulfed red fluorescein were detected by microscopy and analyzed by IMARIS software (lower panel). **B** Bioparticles engulfed in each cell were quantified and compared. multi/n means divided by the number of nuclei in multinucleated microglia (n = 4 per group). **C** Mononuclear and multinucleated microglia were separated by fluorescence-activated cell sorting (FACS) and treated pHrodo-Red *E. coli* for 30 min. **D**, **E** Sorted Cells were labeled with pHrodo Red *E. coli* BioParticles for the indicated time and fluorescein was measured by fluorescence detector (n = 8 per group). On 4-h incubation with BioParticles, fluorescein intensity was indicated in bar graph. **F** CCK-8 assay was used to measure the proliferation of each type of microglia. Sorted cells were incubated for 24 h and proliferation assay were conducted (n = 4 per group). Values are mean ± SD. *: $p < 0.05$; **: $p < 0.01$; ***: p-value < 0.001; ****: p-value < 0.0001

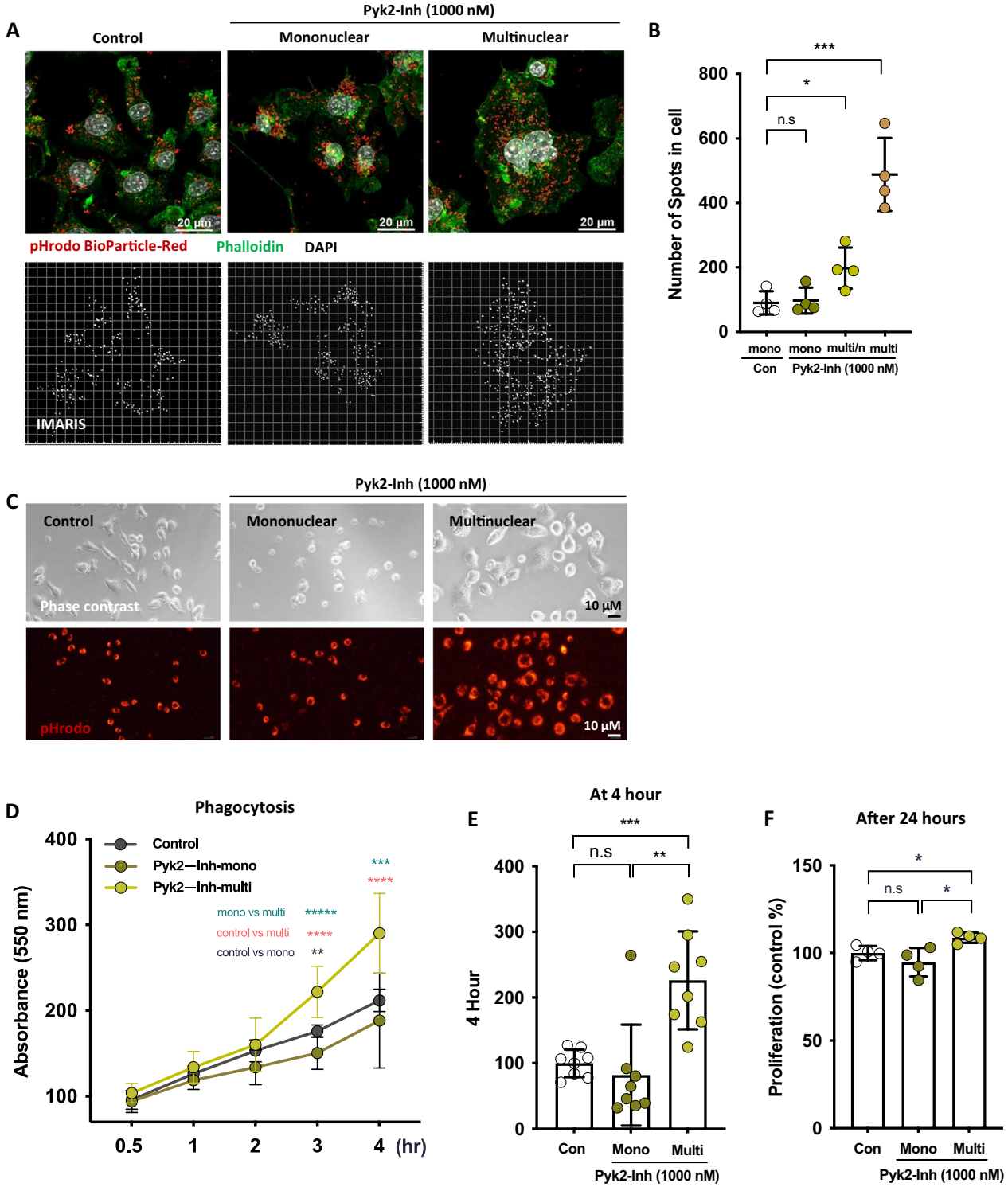

Fig. 3 (See legend on previous page.)

to the naïve control or Pyk2-Inh-mononuclear microglia, assuming that their cell size is larger than that of mononuclear cells. In contrast, mononucleated microglia treated with Pyk2-Inh showed no significant proliferation alteration.

Microglia treated with Pyk2-Inh demonstrate normal lysosomal activity in response to soluble Aβ species

An increase in phagocytic activity was observed following Pyk2-Inh treatment, particularly in multinucleated microglia. Subsequently, we assessed whether phagocytosed soluble Aβ species could be effectively degraded by measuring lysosomal activity. Microglia treated with Pyk2-Inh were additionally exposed to an AD-relevant substrate, Aβ peptides (1–42, 500 ng/mL). After 24 h, both control and Pyk2-Inh treated microglia cells were harvested, lysed, and subjected to immunoblotting to measure the relative protein levels of phosphorylated Pyk2, Lamp1, and phosphorylated Erk (Fig. 4A and B). Exposure to Aβ significantly increased the phosphorylation of Pyk2 (ratio 1.34 ± 0.29 to 4.43 ± 1.25-fold) and reduced Lamp1 expression (ratio 2.69 ± 0.57 to 1.59 ± 0.37-fold) under CSF1 presence, indicating a suppression of lysosomal activity in microglia (Fig. 4A and B). Interestingly, Pyk2 phosphorylation was suppressed by Pyk2-Inh treatment (ratio 4.43 ± 1.25 to 0.45 ± 0.11-fold), and Lamp1 expression levels were significantly restored following treatment with Pyk2-Inh (ratio 1.59 ± 0.37 to 2.92 ± 0.54-fold). Similar to Fig. 1E, the phosphorylation of Erk increased with or without Aβ peptides under Pyk2-Inh treatment. To visualize amyloid phagocytosis, microglia cells were treated with HiLyte-555 labelled $A\beta_{42}$ (500 ng/mL). It was observed that microglia treated with Pyk2-Inh exhibited enhanced phagocytic activity and higher affinity for amyloid peptide. Quantitative analysis showed that the Pyk2-Inh (1000 nM) treated group engulfed more $A\beta_{42}$ spots (average of 16.2 per cell) compared to the control group (average of 5.7 per cell) (Fig. 4C and D). Additionally, to confirm lysosomal activity, we performed a fluorescence dequenching assay using DQ™ Green BSA to assess protease function (Fig. 4E and F). After administered with DQ green BSA for 3 h, intracellular accumulation of fluorescein derivatives (green) was observed (Fig. 4E). In the group treated with Pyk2-Inh (1000 nM), fluorescence intensity of dequenched BODIPY significantly increased compared to control group, indicating higher lysosomal activity (Fig. 4F).

The sorted cells were further analyzed for the transcription levels of phagocytosis-related receptors, such as *Trem2, Cd36* and *Cd74*, along with the phagocytosis substrate gene, *Apoe* (Fig. 4G). In multinucleated microglia treated with Pyk2-Inh, *Trem2* and *Cd36* exhibited significant up-regulation, with 1.9-fold and 3.1-fold increases in transcriptional levels, respectively, whereas *Cd74* and *Apoe* were down-regulated. The transcript level of CD33, a gene associated with LOAD risk and known to inhibits Aβ phagocytosis, was reduced in Pyk2-Inh-mono but comparable to Pyk2-Inh-multinucleated cells when compared to control group. Collectively, our findings indicate that Pyk2 inhibition not only amplifies phagocytosis in microglia—particularly in multinucleated ones—but also enhances the lysosomal activity and the degradation of phagocytosed substrates within these cells.

Morphological changes in microglia observed in the brains of Iba-1 EGFP Tg mice

To examine the in vivo microglial response to Pyk2-Inh, we established an acute Aβ accumulation model using Iba1-EGFP Tg mice as illustrated in Fig. 5A. Pyk2-Inh and HiLyte-555 labelled $A\beta_{42}$ were delivered into the mouse brain through a brain infusion kit connected to an osmotic pump. After 72 h of infusion, the Pyk2-Inh treated group exhibited distinct morphological changes—enlarged cell bodies and shortened ramification—compared to typical naïve microglia, which have thin and elongated ramification (Fig. 5B). Morphological changes were quantitatively analyzed using IMARIS software. In the Pyk2-Inh treated group compared to the control group, cell surface area (μm^2) significantly increased from 103.322 to 267.263, while ramification volume (μm^3) and length (μm) decreased from 2.11 to

(See figure on next page.)

Fig. 4 Pyk2 inhibition stimulates β-amyloid-induced phagocytotic function in multinucleated microglia. **A** Immunoblot of microglia cells after treatment with 1000 nM Pyk2-Inh and 500 ng/mL β-amyloid oligomers (1–42). Cells were treated with 100 ng/mL CSF-1 and 1000 nM Pyk2-Inh for 24 h. Cell lysates were subjected to immunoblotting of p-Pyk2/Pyk2, Lamp1 and p-Erk/Erk. Tubulin was used as a loading control. **B** The quantification of immunoblotting data measured by ImageJ. The same experiments were repeated three times. All full-length uncropped original western blots are included in a Sup. Fig. 5. #: significance between negative control (without CSF1) and control (with CSF1) under β-amyloid absence, #: $p < 0.05$; ##: $p < 0.01$; *: significance between control (with CSF1) and Pyk2-Inh (with CSF1) under β-amyloid presence, *: $p < 0.05$; **: $p < 0.01$; ns; not significant. **C** Immunocytochemical imaging depicted phagocytosis of Aβ (1–42, 500 ng/mL)-Fluor 555 (red) labeled oligomers by microglia cells after exposure to Pyk2-Inh. Cells were stained with anti-Iba1 (cyan) and nuclear DNA was stained with DAPI (white). Scale bar is 20 μm. **D** The quantification of number of spots per cell. After obtaining three-dimensional images, β-amyloid are quantified by a spot analysis using ImageJ. **E** Lysosomal function was assessed using DQ™ Green BSA. Intracellular accumulation of fluorescein derivatives (green) was observed. Scale bar is 100 μm. **F** Fluorescence intensities of dequenched BODIPY resulting from proteolysis activity were measured using a fluorescence plate reader. **G** The transcriptional expression of *Trem2, Cd36, Cd74* and *Apoe* in control and Pyk2 inhibitor treated group in microglia cells. Values are mean ± SD. *: $p < 0.05$; **: $p < 0.01$; ***: p-value < 0.001; ****: p-value < 0.0001

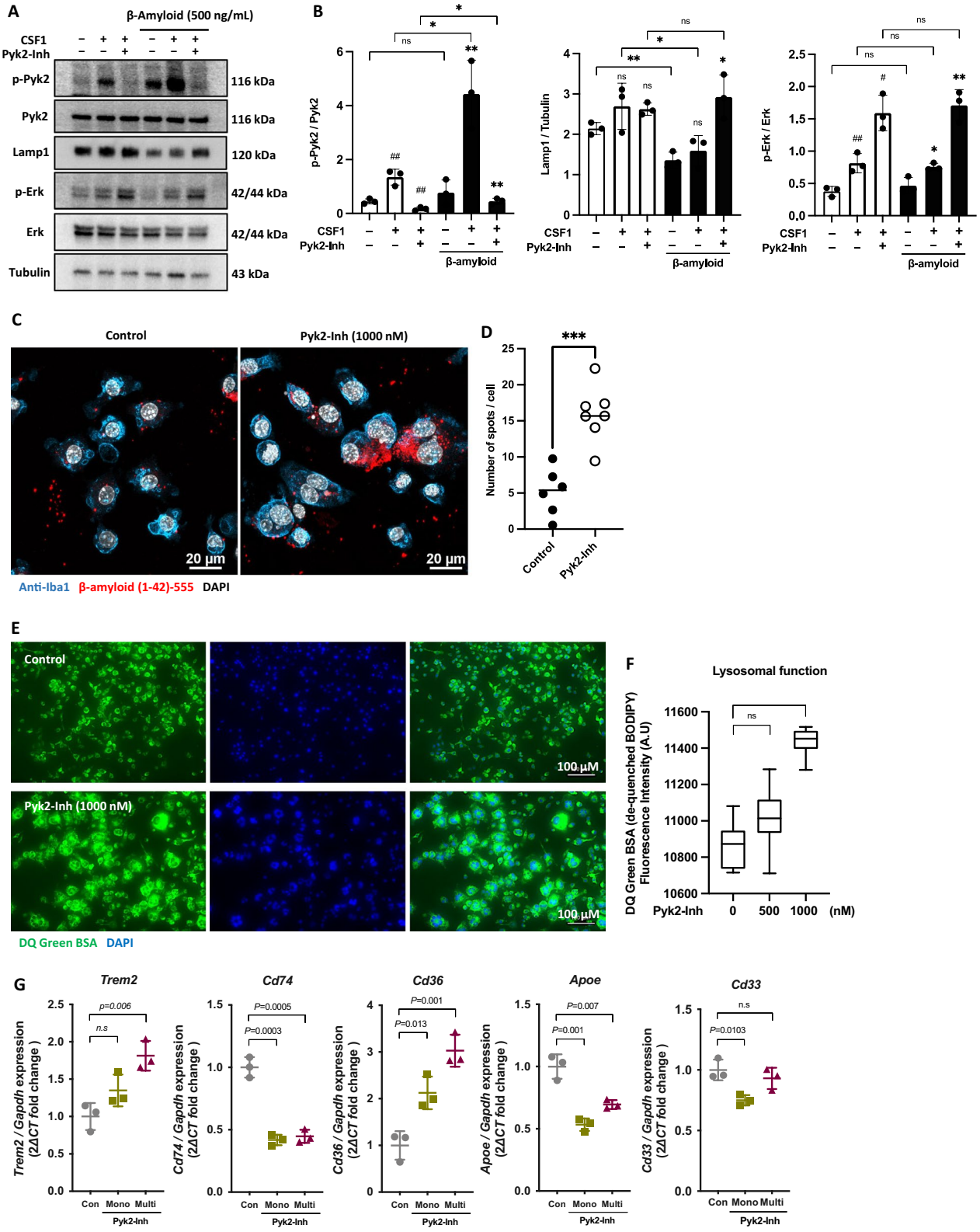

Fig. 4 (See legend on previous page.)

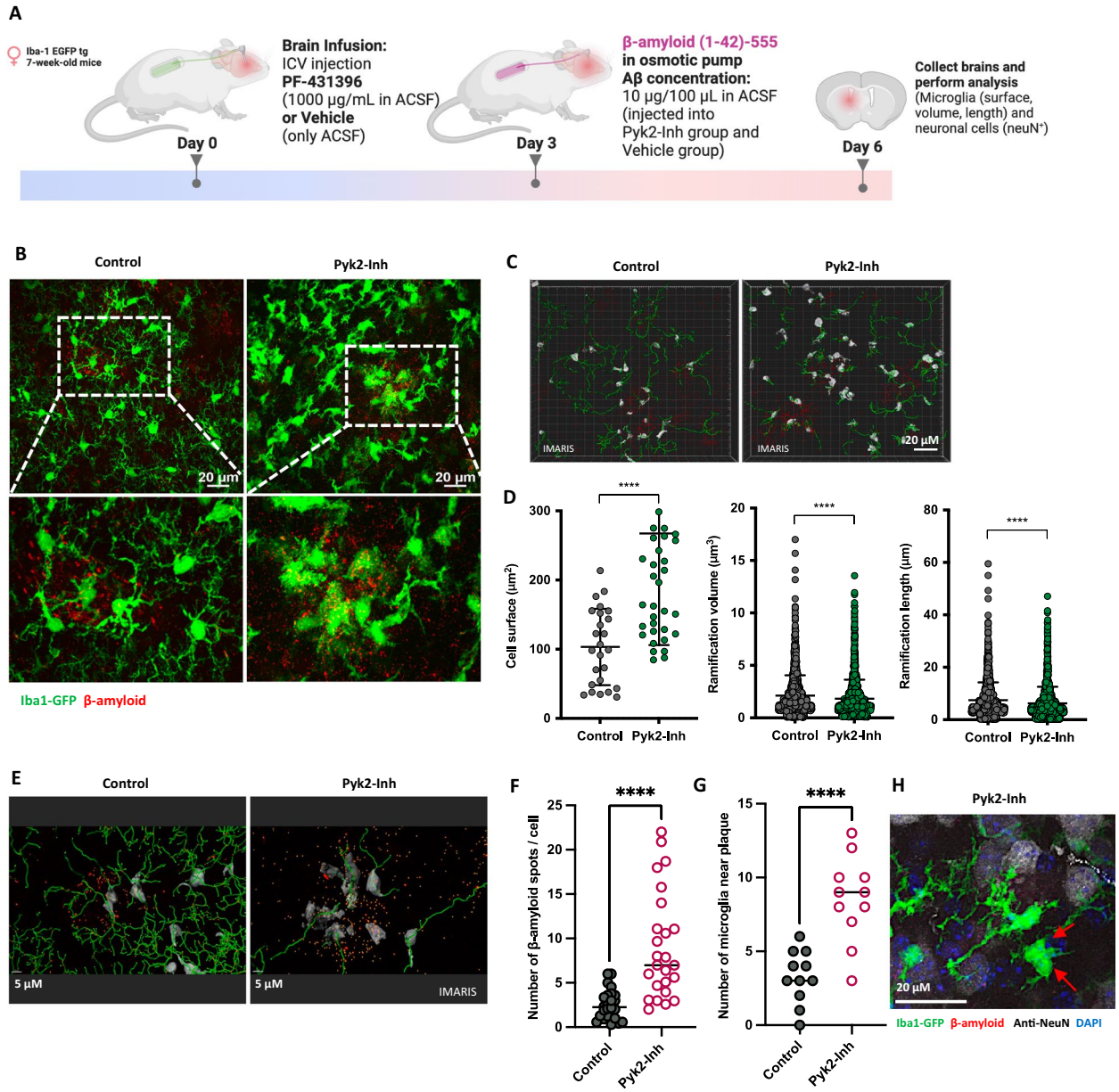

Fig. 5 Altered morphological features and phagocytic function in microglia of Iba-1 EGFP Tg mice brain after Pyk2-Inh infusion. **A** The experimental schedule for brain infusion assay in Iba1-EGFP Tg 7-week-old mice (n = 3/group). **B** Confocal images of GFP positive microglia (green) and β-amyloid (red). Obtained brain slices (thickness ≤ 1.0 mm) were treated with RapiClear 1.52 for tissue clearing and immunohistochemical assay was conducted. **C**, **D** Morphological changes were analyzed by IMARIS software. Cell surface, dendrite volume, and dendrite length were quantified. **E** Spot analysis by IMARIS software. **F**, **G** Quantification of the number of β-amyloid spots per cell and number of microglia deposits. **H** Representative confocal image of multinucleated microglia (indicated red arrow). Brain slices were stained with anti-NeuN (white) and nuclear DNA was stained with DAPI (white). Values are mean ± SD. *: $p < 0.05$; **: $p < 0.01$; ***: p-value < 0.001; ****: p-value < 0.0001

1.78 and from 7.43 to 6.22, respectively (Fig. 5C and D). Surprisingly, compared to controls, Pyk2-Inh-treated microglia showed increased association with amyloid spots (Fig. 5E, marked by orange spots). The quantification of yellow fluorescence, which represents the merge of green and red signal and serves an indicative for internalized Aβ42, revealed a significantly higher density of Aβ spots per cell in the Pyk2-Inh-treated group compared to the control group (6.99 for Pyk2-Inh-treated vs. 2.27 for control). Additionally, there was an increased presence of microglia surrounding the Aβ deposits in the Pyk2-Inh-treated group compared to the control group

(9 for Pyk2-Inh-treated vs. 3 for control) (Fig. 5F and G). We also occasionally observed the multinucleated microglia in the brain tissue (Fig. 5H). These were quantified as ratio of multinucleated microglia per mononuclear microglia from each brain section (Sup. Figure 2A and B). We identified microglia as Iba1-EGFP-positive cells in brain sections, and defied multinucleated microglia as those merged with DAPI-positive staining. Quantification was performed by assessing the proportion of multinucleated microglia among the total microglia count in the imaging. The results showed that the total microglia count was 42 ± 6.67 in the control group and 44.2 ± 7.46 in the Pyk2-Inh treated group, with proportion of multinucleated microglia being 0.017 ± 0.016 in the control group and 0-0.08 ± 0.019 in the Pyk2-Inh treated group. This indicates a 4.56-fold increase in multinucleated microglia observed in the brain tissue due to Py2-Inh treatment compared to the control. In addition, we performed the immunohistochemistry for NeuN, which is specific marker for neurons. The total count of NeuN-positive cells was quantified (Sup. Figure 2C and D). Although Py2-Inh induced multinucleated microglia in mouse brain tissue, the number of neurons was comparable to the control group. This suggests that Pyk2 inhibition could be an effective approach to improve Aβ clearance by enhancing microglial phagocytosis and lysosomal functions without being detrimental to neurons.

Pyk2 inhibition attenuates LPS-induced inflammatory responses of microglia

Given the varying translatability of murine AD data to the actual human disease, we proceeded to investigate the human microglia cell line, HMC3. Initially, we examined whether a Pyk2 inhibitor induces multinucleation in human microglia. As depicted in Sup. Figure 3A, we observed a significant increase in microglia with two or more nuclei, with percentages of 14.47% at 500 nM and 23.27% at 1000 nM of the Pyk2-Inh, compared to 7.43% in the control group (Sup. Figure 3B). Activated microglia play a complex role in neurodegenerative diseases, acting as both beneficial immune responders and detrimental inflammatory mediators. Next, we examined the inflammatory response using HMC3 cells. We pre-treated human microglia cells (HMC3) with Pyk2-Inh for 3 h, followed by LPS stimulation for another 3 h. LPS is frequently used as a stimulus to investigate microglial reactivity and pro-inflammatory responses [60–62]. We then measured their inflammatory responses. Pyk2-Inh treatment significantly reduced the mRNA expression levels of *IL1B, IL6*, and *TNF*, well-characterized inflammatory response genes (Fig. 6A). To corroborate these findings, secreted IL-6 protein levels in the culture medium, measured by ELISA (Fig. 6B), were significantly lower in the Pyk2-Inh-pretreated group compared to the LPS-stimulated control group, consistent with the mRNA level data, further supporting the anti-inflammatory effects of Pyk2 inhibition. Next, we investigated the downstream signaling of LPS stimulation using Western blot analysis (Fig. 6C). The inflammatory mater regulator, NF-kB, is activated by LPS. The phosphorylation of NF-kB rapidly responds to LPS, initiating inflammatory responses. The expression of NF-kB markedly increased 15 min after LPS priming compared to 0 min (from 0.51 ± 0.31 to 1.53 ± 0.35-fold). Conversely, in the presence of Pyk2-Inh, stimulation of microglia by LPS results in decreased expression of NF-kB as early as the 0–5-min time point, significantly decreasing from 1.53 ± 0.35 to 0.92 ± 0.37 at 15 min (Fig. 6D). Thus, the suppression of phosphorylated form of NF-kB due to Pyk2-Inh suggests a reduction in LPS-induced inflammatory responses mediated by NF-kB inhibition.

Discussions

Effective clearance of Aβ oligomers and insoluble fibrils by microglia is important for preventing or slowing down senile plaque formation and other pathophysiological changes in AD. During the preclinical and early stages of AD, activating microglia is crucial for efficient Aβ clearance [63]. Enhanced phagocytosis improves the clearance of pathogens, dead cells, and debris, which is essential for preventing infections and maintaining a healthy neural environment [64]. In contrast, late-stage dysfunction and persistent activation of microglia and enhanced phagocytosis can lead to chronic inflammation. In some cases, overactive phagocytosis can result in the engulfment and destruction of healthy neurons and synapses, contributing to neurodegeneration and cognitive decline [65]. This complex, dual nature of microglia in AD presents challenges in pinpointing targets and demonstrating treatment effectiveness. Therefore, understanding the balance and regulation of microglia phagocytosis is crucial for developing therapeutic strategies for a variety of neurological conditions.

The pathogenesis of AD is multifactorial, involving several key pathological hallmarks: amyloid plaques accumulation, tau protein abnormalities and neuroinflammation [66]. Amyloid plaques are composed of the β-amyloid peptide $A\beta_{1\text{-}42}$, a toxic derivative of the amyloid precursor protein (APP), while neurofibrillary tangles are formed from aggregates of hyperphosphorylated Tau, a microtubule-binding protein. Recent GWAS have identified PTK2B as a susceptibility locus for AD [29–31, 67–69], pointing to the Pyk2 may play a role in the AD pathology. Pyk2 phosphorylation shows heightened activity in wild-type mouse brain slices exposed to Aβ oligomer and in aged *APP^{swe}/PS1ΔE9* transgenic mouse

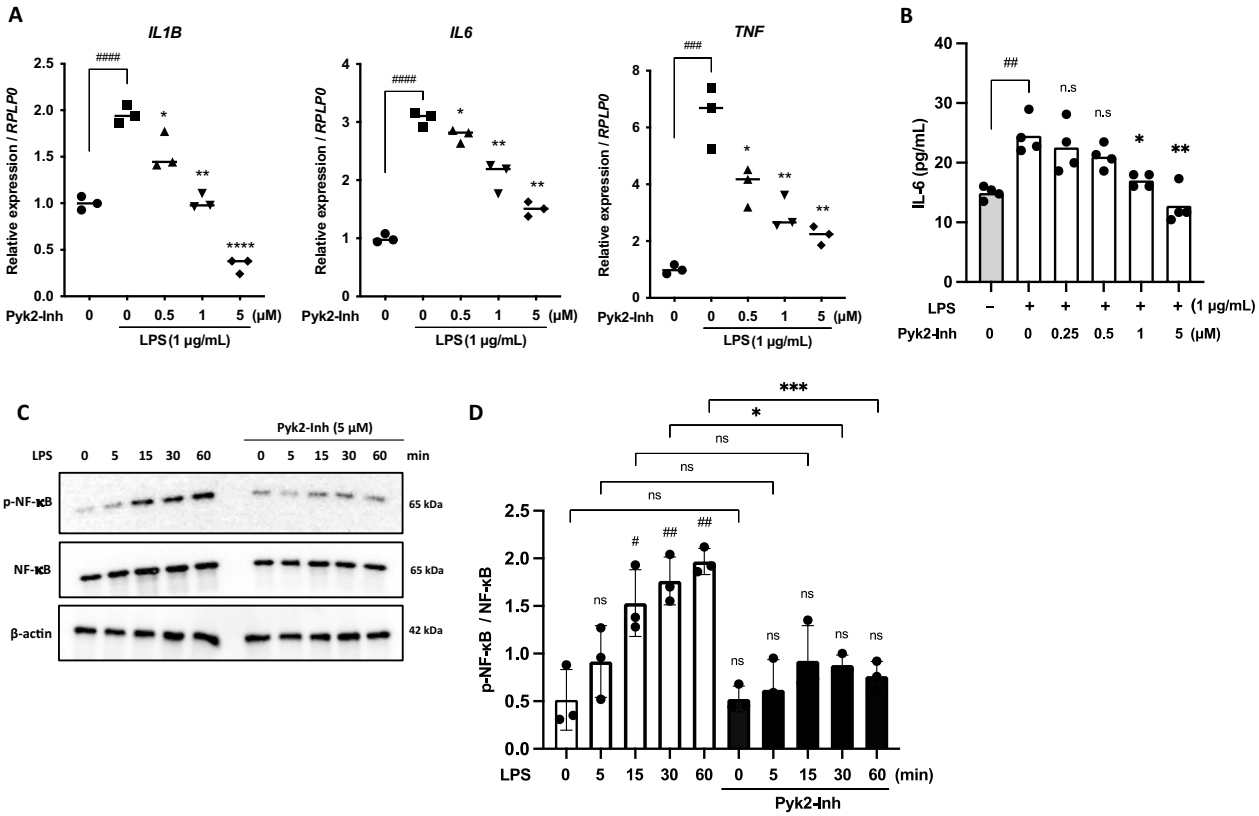

Fig. 6 Pyk2 inhibition reduces LPS-induced inflammation in human microglia. **A** The transcriptional expression of *IL1β, IL6* and *TNF* in control and Pyk2-Inh treated group in human microglia cells, HMC3. **B** The secreted protein level of IL-6 was measured by ELISA. **C** The time-course Immunoblotting images of phosphor-NF-kB and NF-kB in HMC3 cells after LPS stimulation and with or without Pyk2-Inh. β-actin was used for loading control. The same experiments were repeated three times. **D** Quantification of immunoblotting data was measured by ImageJ. All full-length uncropped original western blots are included in a Sup. Fig. 6. Values are mean ± SD. #: significance between negative control and LPS control, #: $p < 0.05$; ##: $p < 0.01$; *: significance between LPS control and Pyk2-Inh treated groups, *: $p < 0.05$; **: $p < 0.01$; ***: $p < 0.001$; ns: not significant

brain [70, 71]. Pyk2 is part of a signaling cascade triggered by oligomeric Aβ (Aβo) [72]. This cascade involves the cellular prion protein (PrPc), which act as a receptor of Aβo, and interacts with mGluR5, Homer1b/c, Pyk2, and Ca^{2+}/calmodulin-dependent protein kinase II [70]. These cascade phosphorylated Tau, potentially facilitating its aggregation and the formation of neurofibrillary tangles. The absence of Pyk2 exacerbates mutant Tau-dependent phenotypes in PS19 mice, partly due to increased LKB1 and MAPK activity [73]. These data suggest that while Pyk2 activity mediates Aβ-driven deficits AD, it also suppresses Tau-related phenotypes. Additionally, Pyk2 KO also improves dendritic spine loss induced by Aβo, likely by alleviating the inhibition of Graf1c, a RhoA GTPase-activating protein by Pyk2 [74]. Similarly, our results showed that despite the increased phagocytic function of microglia by Pyk2 inhibition, there was no significant difference in the number of neurons measured by the NeuN marker between the control group and Pyk2-Inh treated group. Therefore, Pyk2 inhibition may does not affect neuronal loss. Collectively, these findings indicate that Pyk2 may contribute to tauopathy by directly and indirectly modifying Tau phosphorylation at multiple sites. Thus, Pyk2 is a promising candidate for linking Aβ and tau pathology within the amyloid cascade hypothesis.

In the current study, we developed an assay to assess microglial function, exploring Pyk2-Inh's effects on Aβ clearance. Notably, Pyk2 inhibition induced multinucleated microglia formation, associated with improved phagocytic and proteolytic capabilities. Multinucleated microglia represent a unique and intriguing aspect of microglial biology, frequently associated with severe chronic pathological conditions [75]. These cells are prominently observed in conditions such as HIV/AIDS encephalopathy [75, 76], which suggests their genesis may be attributed to cell fusion processes activated by viral presence within microglia. The formation of

multinucleated cells deviates from the conventional behavior of microglia, which are typically characterized by a territorial disposition and exhibit pronounced contact inhibition, delineated by a slim and extensively branched morphology [77]. The precise biological purpose and consequence of multinucleated microglia formation are yet to be elucidated. These cells may arise through mechanisms such as failed cell division, cell fusion or other forms of cellular stress [76, 78, 79]. Unlike osteoclasts, where multinucleation is irreversible [80], microglial multinucleation is reversible. This raises questions about the functional relevance of this phenomenon. The increased size of multinucleated microglia hints at a potential specialization for enhanced phagocytosis, allowing them to engulf larger cellular debris or particulate matter.

Pyk2 also plays an important role in inflammatory diseases [54, 81]. In vitro, Pyk2 acts downstream of PKC to mediate the secretion of neurotoxic factors by microglia in response to Aβ stimulation [82]. TRPM2, a ROS-sensitive calcium channel expressed in neurons, astrocytes, and microglia, has been linked to numerous neurological diseases [83]. In monocytes (circulating macrophages), TRPM2 activates the Pyk2/ERK pathway, leading to chemokine production and increased inflammation [84]. This pathway is crucial for microglia activation by $A\beta_{1\text{-}42}$, resulting in the release of cytotoxic tumor necrosis factor-α (TNF-α). Pyk2 enhances this process through positive feedback on the TRPM2 channel [85]. In microglia treated with Pyk2-Inh, we observed a significant decrease in LPS-induced inflammatory response, accompanied by decrease of phosphorylated NF-kB and reduced transcriptional expression of inflammatory genes, including *IL1β, IL6,* and *TNF*. This reduction in inflammatory response could be attributed to Pyk2 inhibition potentially interfering with the Pyk2 and MyD88 interaction [42]. MyD88 is essential for linking LPS-activated TLRs with the Pyk2/IRF4 complex [42, 86], underscoring the significance of targeting these interactions in therapeutic strategies designed to enhance Aβ clearance mechanisms in neuroinflammatory and neurodegenerative disorders while simultaneously reducing pro-inflammatory signals.

One limitation of this study is the specificity of the Pyk2 inhibitor, PF-431396. This small molecule inhibitor targets PTK2B, but due to Pyk2's 65% homology and shared domain structure with FAK [87–89], PF-431396 can also inhibit FAK activity, as demonstrated in immunoblot assay (Fig. 1E). Despite this limitation, our research identifies a significant benefit of PF-431396 in triggering multinucleated microglia formation, associated with enhanced phagocytic capabilities. The exclusive enhancement of phagocytic activity in multinucleated microglia treated with PF-431396 underscores the potential significance of Pyk2/FAK pathways in microglial phagocytosis, meriting further exploration. Additionally, ongoing Phase II clinical trials of FAK inhibitors for breast cancer metastasis inhibition [90], and studies on the efficacy of dual Pyk2/FAK inhibitors in such contexts, underscore the broader therapeutic potential of targeting these signaling pathways [91].

There is a critical need for further research to elucidate the mechanisms that Pyk2 plays in diverse AD animal models and to assess their applicability to human diseases. AD genetic mouse models (e.g., *App/Psen1* or 5xFAD) are commonly used to mimic the pathophysiology of AD and evaluate potential therapeutic interventions [92, 93]. However, the fact that we only validated the effects of the Pyk2 inhibitor in an acute AD model and did not assess its efficacy in an AD genetic mouse model raises important consideration for discussion. While acute AD models allow for rapid assessment of therapeutic effects, AD genetic mouse model more closely recapitulate the progressive nature and complexity of AD observed in humans. Therefore, the lack of validation in AD genetic models raises questions about the translational potential of our findings and underscores the need for further investigation in models that better represent the disease phenotype. Lastly, considering alternative models or experimental approaches that better reflect the genetic complexity and progressive nature of AD can enhance the translational relevance of our findings. This may include utilizing transgenic mouse models expressing familial AD mutations or incorporating in vitro models with human-derived cells and genetic variants associated with AD.

Supporting the positive role of Pyk2, studies have shown reduced Tyr402 phosphorylation levels in the hippocampus can be mitigated by overexpressing Pyk2 in this brain region. This overexpression restores autophosphorylated Pyk2 levels, enhances synaptic markers, and improve performance in behavioral tasks, despite a slight increase in plaque number in 5XFAD mice [94]. Furthermore, overexpressing Pyk2 in hippocampal neurons within a microfluidic culture system has been shown to protect these neurons from $A\beta_{1\text{-}42}$ toxicity [95]. Although the precise role of elevated Pyk2 expression in microglia and its contribution to AD pathology has yet to be explored, it is conceivable that Pyk2 significantly modulates microglial activity, neuroinflammatory responses, and synaptic integrity. While inhibition of Pyk2 has been shown to reduce pathological tau phosphorylation and neuroinflammation as discussed in earlier, overexpression studies indicate that Pyk2 may also play a protective role by enhancing synaptic plasticity and neuronal survival. The seemingly contradictory effects of Pyk2

inhibition and overexpression could be attributed to the specific cellular contexts or stages of the disease in which Pyk2 activity is modulated. Additionally, compensatory mechanisms and the precise levels of Pyk2 activity might critically influence the outcomes. Therefore, further studies are required to elucidate the conditions under which Pyk2 inhibition or overexpression can be therapeutically beneficial, take into account the functional diversity and regulatory mechanisms of Pyk2 in AD pathology.

In this study, we found a novel discovery that microglia undergo multinucleation upon inhibition of Pyk2 using PF-431396, and we demonstrated that this multinucleation correlates with an increased ability of the cells to engulf Aβ. Specifically, activated microglia are known to exert phagocytotic activity particularly heightened by inflammation. However, these multinucleated microglia not only do not exacerbate inflammatory responses induced by LPS but also facilitate the clearance of Aβ. Intriguingly, we noted an increased affinity for amyloid spots around Pyk2-Inh-treated microglia, particularly in multinucleated microglia in vitro, and observed enhanced migration of microglia around amyloid deposits in vivo. These findings suggest a potential therapeutic avenue for inflammatory neurodegenerative disorders, where inflammation could be mitigated while promoting Aβ clearance.

Abbreviations

Aβ	β-Amyloid
PTK2B	Protein Tyrosine Kinase 2 Beta
EGFP	Enhanced Green Fluorescent Protein
LPS	Lipopolysaccharide
CNS	Central nervous system
AD	Alzheimer's disease
PD	Parkinson's disease
MS	Multiple sclerosis
LOAD	Late-onset Alzheimer's disease
FAK	Focal adhesion kinase
GWAS	Genome-wide association study
ICV	Intracerebroventricular
Tg	Transgenic
ACSF	Artificial cerebrospinal fluid
FACS	Fluorescence-activated cell sorting

Supplementary Information

The online version contains supplementary material available at https://doi.org/10.1186/s12974-024-03192-7.

Additional file 1: Figure 1 Fluorescence-activated cell sorting (FACS) Gating strategy. The gating strategy for FACS aimed to isolate the mononucleated cells and multinucleated cells. MG6 cells were stained with Hoechst 33342 for 5 minutes before being loaded into the FACS. Following the exclusion of the cell debris and doublet cells, the remaining cells were segregated based on size differences, with P4 representing mononucleated cells and P5 representing multinucleated cells. Figure 2 Analysis of multinucleated microglia and NeuN-positive cells in mouse brain tissue. A) Iba1-EGFP positive microglia (green) were visualized and merged with DAPI staining (blue). Microglia with two or more nuclei per cell were classified as multinucleated. Red arrows indicated the multinucleated microglia. B) The data is presented as the ratio of multinucleated to mononucleated microglia (control=5, Pyk2-Inh=5). C) Representative images of immunofluorescence staining for anti-NeuN (white). D) The total count of NeuN-positive cells was quantified (control=7, Pyk2-Inh=7). Figure 3 Pyk2 inhibition induces multinucleation in human microglia cells. HMC3 cells were seeded at a density of 1 X 10^4 cells per well in a 96-well plate and incubated with or without Pyk2-Inh at concentrations of 500 and 1000 nM. A) After 24 hours, the cells were fixed with 10% formalin and stained with phalloidin (red) for the cytoskeleton and DAPI (blue) for nuclei. B) Microglia with two or more nuclei per cell were classified as multinucleated Yellow arrows indicated the multinucleated microglia. (control=5, Pyk2-Inh 500 nM=5, Pyk2-Inh-1000 nM=5). The experiments were repeated three times. Figure 4 All full-length uncropped original western blots from Fig. 1E. Figure 5. All full-length uncropped original western blots from Fig. 4A. Figure 6. All full-length uncropped original western blots from Fig. 6C. Movie 1. Cell division in the control group by time-lapse video microscopy. Nuclei were stained with Hoechst 33342 staining. Movie 2. Cell division in Pyk2-Inh treated group by time-lapse video microscopy. Nuclei were stained with Hoechst 33342 staining. Movie 3. Morphological feature analysis of control microglia by IMARIS. Movie 4. Morphological feature analysis of Pyk2-Inh treated microglia by IMARIS. Table 1 Oligonucleotide primer sequence for RT-qPCR.

Author contributions

J-W.L. and S.W.K conceived the study, and wrote the manuscript; J-W.L. designed the experiments and K.M., H.W., and T.T. performed the experiments. I-H. L performed the data interpretation. K.H., Y.Y., Y.K., A.H. and T.I. provided insightful discussion. S.W.K. supervised the project. All authors approved the final manuscript.

Funding

This work was supported by Grant-in-Aids for Scientific Research from the Japan Society for the Promotion of Science (JSPS KAKENHI) grant number 23K09116, the Takeda Science Foundation, and the JSBMR Rising Star Grant, which were awarded to J-W. L. This work was partly supported by the National Institute of Health (Grand numbers: R01NS129188 and U01TR002623) to S.W.K.

Availability of data and materials

No datasets were generated or analyzed during the current study.

Declarations

Ethics approval and consent to participate

Experiments using mice were approved by the Institutional animal care and use committee of Hokkaido University, Japan and were performed in accordance with the committee's guiding principle (approval no.: 21-0018).

Competing interests

The authors declare no competing interests.

Received: 7 June 2024 Accepted: 31 July 2024
Published online: 06 August 2024

References

1. McKhann GM, Knopman DS, Chertkow H, Hyman BT, Jack CR Jr, Kawas CH, Klunk WE, Koroshetz WJ, Manly JJ, Mayeux R, et al. The diagnosis of dementia due to Alzheimer's disease: recommendations from the national institute on aging-Alzheimer's association workgroups on diagnostic guidelines for Alzheimer's disease. Alzheimers Dement. 2011;7:263–9.
2. Braak H, Braak E. Neuropathological stageing of Alzheimer-related changes. Acta Neuropathol. 1991;82:239–59.
3. Hur JY. gamma-Secretase in Alzheimer's disease. Exp Mol Med. 2022;54:433–46.

4. Bertram L, Tanzi RE. Thirty years of Alzheimer's disease genetics: the implications of systematic meta-analyses. Nat Rev Neurosci. 2008;9:768–78.
5. Coric V, van Dyck CH, Salloway S, Andreasen N, Brody M, Richter RW, Soininen H, Thein S, Shiovitz T, Pilcher G, et al. Safety and tolerability of the gamma-secretase inhibitor avagacestat in a phase 2 study of mild to moderate Alzheimer disease. Arch Neurol. 2012;69:1430–40.
6. Egan MF, Kost J, Tariot PN, Aisen PS, Cummings JL, Vellas B, Sur C, Mukai Y, Voss T, Furtek C, et al. Randomized trial of verubecestat for mild-to-moderate Alzheimer's disease. N Engl J Med. 2018;378:1691–703.
7. Fleisher AS, Raman R, Siemers ER, Becerra L, Clark CM, Dean RA, Farlow MR, Galvin JE, Peskind ER, Quinn JF, et al. Phase 2 safety trial targeting amyloid beta production with a gamma-secretase inhibitor in Alzheimer disease. Arch Neurol. 2008;65:1031–8.
8. May PC, Dean RA, Lowe SL, Martenyi F, Sheehan SM, Boggs LN, Monk SA, Mathes BM, Mergott DJ, Watson BM, et al. Robust central reduction of amyloid-beta in humans with an orally available, non-peptidic beta-secretase inhibitor. J Neurosci. 2011;31:16507–16.
9. Siemers ER, Quinn JF, Kaye J, Farlow MR, Porsteinsson A, Tariot P, Zoulnouni P, Galvin JE, Holtzman DM, Knopman DS, et al. Effects of a gamma-secretase inhibitor in a randomized study of patients with Alzheimer disease. Neurology. 2006;66:602–4.
10. Wessels AM, Lines C, Stern RA, Kost J, Voss T, Mozley LH, Furtek C, Mukai Y, Aisen PS, Cummings JL, et al. Cognitive outcomes in trials of two BACE inhibitors in Alzheimer's disease. Alzheimers Dement. 2020;16:1483–92.
11. Podlesny-Drabiniok A, Marcora E, Goate AM. Microglial phagocytosis: a disease-associated process emerging from Alzheimer's disease genetics. Trends Neurosci. 2020;43:965–79.
12. Baik SH, Kang S, Son SM, Mook-Jung I. Microglia contributes to plaque growth by cell death due to uptake of amyloid beta in the brain of Alzheimer's disease mouse model. Glia. 2016;64:2274–90.
13. Doens D, Fernandez PL. Microglia receptors and their implications in the response to amyloid beta for Alzheimer's disease pathogenesis. J Neuroinflammation. 2014;11:48.
14. Paolicelli RC, Bolasco G, Pagani F, Maggi L, Scianni M, Panzanelli P, Giustetto M, Ferreira TA, Guiducci E, Dumas L, et al. Synaptic pruning by microglia is necessary for normal brain development. Science. 2011;333:1456–8.
15. Gomez-Nicola D, Fransen NL, Suzzi S, Perry VH. Regulation of microglial proliferation during chronic neurodegeneration. J Neurosci. 2013;33:2481–93.
16. Koenigsknecht J, Landreth G. Microglial phagocytosis of fibrillar beta-amyloid through a beta1 integrin-dependent mechanism. J Neurosci. 2004;24:9838–46.
17. Sasaki A, Yamaguchi H, Ogawa A, Sugihara S, Nakazato Y. Microglial activation in early stages of amyloid beta protein deposition. Acta Neuropathol. 1997;94:316–22.
18. Liu B. Modulation of microglial pro-inflammatory and neurotoxic activity for the treatment of Parkinson's disease. AAPS J. 2006;8:E606-621.
19. Long-Smith CM, Sullivan AM, Nolan YM. The influence of microglia on the pathogenesis of Parkinson's disease. Prog Neurobiol. 2009;89:277–87.
20. Hill KE, Zollinger LV, Watt HE, Carlson NG, Rose JW. Inducible nitric oxide synthase in chronic active multiple sclerosis plaques: distribution, cellular expression and association with myelin damage. J Neuroimmunol. 2004;151:171–9.
21. Mack CL, Vanderlugt-Castaneda CL, Neville KL, Miller SD. Microglia are activated to become competent antigen presenting and effector cells in the inflammatory environment of the Theiler's virus model of multiple sclerosis. J Neuroimmunol. 2003;144:68–79.
22. Rose JW, Hill KE, Watt HE, Carlson NG. Inflammatory cell expression of cyclooxygenase-2 in the multiple sclerosis lesion. J Neuroimmunol. 2004;149:40–9.
23. Krasemann S, Madore C, Cialic R, Baufeld C, Calcagno N, El Fatimy R, Beckers L, O'Loughlin E, Xu Y, Fanek Z, et al. The TREM2-APOE pathway drives the transcriptional phenotype of dysfunctional microglia in neurodegenerative diseases. Immunity. 2017;47:566-581 e569.
24. Norris GT, Smirnov I, Filiano AJ, Shadowen HM, Cody KR, Thompson JA, Harris TH, Gaultier A, Overall CC, Kipnis J. Neuronal integrity and complement control synaptic material clearance by microglia after CNS injury. J Exp Med. 2018;215:1789–801.
25. Fu AK, Hung KW, Yuen MY, Zhou X, Mak DS, Chan IC, Cheung TH, Zhang B, Fu WY, Liew FY, Ip NY. IL-33 ameliorates Alzheimer's disease-like pathology and cognitive decline. Proc Natl Acad Sci U S A. 2016;113:E2705-2713.
26. Lee CYD, Daggett A, Gu X, Jiang LL, Langfelder P, Li X, Wang N, Zhao Y, Park CS, Cooper Y, et al. Elevated TREM2 gene dosage reprograms microglia responsivity and ameliorates pathological phenotypes in Alzheimer's disease models. Neuron. 2018;97:1032-1048 e1035.
27. Nolte C, Moller T, Walter T, Kettenmann H. Complement 5a controls motility of murine microglial cells in vitro via activation of an inhibitory G-protein and the rearrangement of the actin cytoskeleton. Neuroscience. 1996;73:1091–107.
28. Uhlemann R, Gertz K, Boehmerle W, Schwarz T, Nolte C, Freyer D, Kettenmann H, Endres M, Kronenberg G. Actin dynamics shape microglia effector functions. Brain Struct Funct. 2016;221:2717–34.
29. Kunkle BW, Grenier-Boley B, Sims R, Bis JC, Damotte V, Naj AC, Boland A, Vronskaya M, van der Lee SJ, Amlie-Wolf A, et al. Genetic meta-analysis of diagnosed Alzheimer's disease identifies new risk loci and implicates Abeta, tau, immunity and lipid processing. Nat Genet. 2019;51:414–30.
30. Lambert JC, Ibrahim-Verbaas CA, Harold D, Naj AC, Sims R, Bellenguez C, DeStafano AL, Bis JC, Beecham GW, Grenier-Boley B, et al. Meta-analysis of 74,046 individuals identifies 11 new susceptibility loci for Alzheimer's disease. Nat Genet. 2013;45:1452–8.
31. Beecham GW, Hamilton K, Naj AC, Martin ER, Huentelman M, Myers AJ, Corneveaux JJ, Hardy J, Vonsattel JP, Younkin SG, et al. Genome-wide association meta-analysis of neuropathologic features of Alzheimer's disease and related dementias. PLoS Genet. 2014;10: e1004606.
32. Jiao B, Liu X, Zhou L, Wang MH, Zhou Y, Xiao T, Zhang W, Sun R, Waye MM, Tang B, Shen L. Polygenic analysis of late-onset Alzheimer's disease from Mainland China. PLoS ONE. 2015;10: e0144898.
33. Lawingco T, Chaudhury S, Brookes KJ, Guetta-Baranes T, Guerreiro R, Bras J, Hardy J, Francis P, Thomas A, Belbin O, Morgan K. Genetic variants in glutamate-, Abeta-, and tau-related pathways determine polygenic risk for Alzheimer's disease. Neurobiol Aging. 2021;101:299 e213-299 e221.
34. Nettiksimmons J, Tranah G, Evans DS, Yokoyama JS, Yaffe K. Gene-based aggregate SNP associations between candidate AD genes and cognitive decline. Age (Dordr). 2016;38:41.
35. Wang X, Lopez O, Sweet RA, Becker JT, DeKosky ST, Barmada MM, Feingold E, Demirci FY, Kamboh MI. Genetic determinants of survival in patientswith Alzheimer's disease. J Alzheimers Dis. 2015;45:651–8.
36. Menegon A, Burgaya F, Baudot P, Dunlap DD, Girault JA, Valtorta F. FAK+ and PYK2/CAKbeta, two related tyrosine kinases highly expressed in the central nervous system: similarities and differences in the expression pattern. Eur J Neurosci. 1999;11:3777–88.
37. Zhang C, Lambert MP, Bunch C, Barber K, Wade WS, Krafft GA, Klein WL. Focal adhesion kinase expressed by nerve cell lines shows increased tyrosine phosphorylation in response to Alzheimer's A beta peptide. J Biol Chem. 1994;269:25247–50.
38. Schaller MD. Calcium-dependent Pyk2 activation: a role for calmodulin? Biochem J. 2008;410:e3-4.
39. Shen CJ, Raghavan S, Xu Z, Baranski JD, Yu X, Wozniak MA, Miller JS, Gupta M, Buckbinder L, Chen CS. Decreased cell adhesion promotes angiogenesis in a Pyk2-dependent manner. Exp Cell Res. 2011;317:1860–71.
40. Rolon-Reyes K, Kucheryavykh YV, Cubano LA, Inyushin M, Skatchkov SN, Eaton MJ, Harrison JK, Kucheryavykh LY. Microglia activate migration of glioma cells through a Pyk2 intracellular pathway. PLoS ONE. 2015;10: e0131059.
41. Hide I, Shiraki H, Masuda A, Maeda T, Kumagai M, Kunishige N, Yanase Y, Harada K, Tanaka S, Sakai N. P2Y(2) receptor mediates dying cell removal via inflammatory activated microglia. J Pharmacol Sci. 2023;153:55–67.
42. Xi CX, Xiong F, Zhou Z, Mei L, Xiong WC. PYK2 interacts with MyD88 and regulates MyD88-mediated NF-kappaB activation in macrophages. J Leukoc Biol. 2010;87:415–23.
43. Naser R, Aldehaiman A, Diaz-Galicia E, Arold ST. Endogenous control mechanisms of FAK and PYK2 and their relevance to cancer development. Cancers. 2018;10:96.
44. Mastrolia V, Al Massadi O, de Pins B, Girault JA. Pyk2 in dorsal hippocampus plays a selective role in spatial memory and synaptic plasticity. Sci Rep. 2021;11:16357.
45. Salazar SV, Cox TO, Lee S, Brody AH, Chyung AS, Haas LT, Strittmatter SM. Alzheimer's Disease risk factor Pyk2 mediates amyloid-beta-induced synaptic dysfunction and loss. J Neurosci. 2019;39:758–72.

46. Bartos JA, Ulrich JD, Li H, Beazely MA, Chen Y, Macdonald JF, Hell JW. Postsynaptic clustering and activation of Pyk2 by PSD-95. J Neurosci. 2010;30:449–63.
47. Guo Y, Sun CK, Tang L, Tan MS. Microglia PTK2B/Pyk2 in the pathogenesis of Alzheimer's disease. Curr Alzheimer Res. 2024;20:692–704.
48. Johnson RD, Schauerte JA, Wisser KC, Gafni A, Steel DG. Direct observation of single amyloid-beta(1–40) oligomers on live cells: binding and growth at physiological concentrations. PLoS ONE. 2011;6: e23970.
49. Ryan TM, Caine J, Mertens HD, Kirby N, Nigro J, Breheney K, Waddington LJ, Streltsov VA, Curtain C, Masters CL, Roberts BR. Ammonium hydroxide treatment of Abeta produces an aggregate free solution suitable for biophysical and cell culture characterization. PeerJ. 2013;1: e73.
50. Condello C, Yuan P, Schain A, Grutzendler J. Microglia constitute a barrier that prevents neurotoxic protofibrillar Abeta42 hotspots around plaques. Nat Commun. 2015;6:6176.
51. Taylor ZV, Khand B, Porgador A, Monsonego A, Eremenko E. An optimized intracerebroventricular injection of CD4(+) T cells into mice. STAR Protoc. 2021;2:100725.
52. Loryan I, Friden M, Hammarlund-Udenaes M. The brain slice method for studying drug distribution in the CNS. Fluids Barriers CNS. 2013;10:6.
53. Pai KS, Shankar SK, Ravindranath V. A simple and inexpensive slicer for preparation of brain slices. J Neurosci Methods. 1991;37:209–14.
54. Okigaki M, Davis C, Falasca M, Harroch S, Felsenfeld DP, Sheetz MP, Schlessinger J. Pyk2 regulates multiple signaling events crucial for macrophage morphology and migration. Proc Natl Acad Sci U S A. 2003;100:10740–5.
55. Imai Y, Kohsaka S. Intracellular signaling in M-CSF-induced microglia activation: role of Iba1. Glia. 2002;40:164–74.
56. Marzolo MP, von Bernhardi R, Inestrosa NC. Mannose receptor is present in a functional state in rat microglial cells. J Neurosci Res. 1999;58:387–95.
57. Cao LG, Wang YL. Mechanism of the formation of contractile ring in dividing cultured animal cells. II. Cortical movement of microinjected actin filaments. J Cell Biol. 1990;111:1905–11.
58. Bornens M. The centrosome in cells and organisms. Science. 2012;335:422–6.
59. Wong C, Stearns T. Centrosome number is controlled by a centrosome-intrinsic block to reduplication. Nat Cell Biol. 2003;5:539–44.
60. Wang X, Rousset CI, Hagberg H, Mallard C. Lipopolysaccharide-induced inflammation and perinatal brain injury. Semin Fetal Neonatal Med. 2006;11:343–53.
61. Lund S, Christensen KV, Hedtjarn M, Mortensen AL, Hagberg H, Falsig J, Hasseldam H, Schrattenholz A, Porzgen P, Leist M. The dynamics of the LPS triggered inflammatory response of murine microglia under different culture and in vivo conditions. J Neuroimmunol. 2006;180:71–87.
62. Hoogland IC, Houbolt C, van Westerloo DJ, van Gool WA, van de Beek D. Systemic inflammation and microglial activation: systematic review of animal experiments. J Neuroinflammation. 2015;12:114.
63. Streit WJ, Xue QS, Tischer J, Bechmann I. Microglial pathology. Acta Neuropathol Commun. 2014;2:142.
64. Salter MW, Stevens B. Microglia emerge as central players in brain disease. Nat Med. 2017;23:1018–27.
65. Hampel H, Hardy J, Blennow K, Chen C, Perry G, Kim SH, Villemagne VL, Aisen P, Vendruscolo M, Iwatsubo T, et al. The amyloid-beta pathway in Alzheimer's disease. Mol Psychiatry. 2021;26:5481–503.
66. DaRocha-Souto B, Scotton TC, Coma M, Serrano-Pozo A, Hashimoto T, Sereno L, Rodriguez M, Sanchez B, Hyman BT, Gomez-Isla T. Brain oligomeric beta-amyloid but not total amyloid plaque burden correlates with neuronal loss and astrocyte inflammatory response in amyloid precursor protein/tau transgenic mice. J Neuropathol Exp Neurol. 2011;70:360–76.
67. Jansen IE, Savage JE, Watanabe K, Bryois J, Williams DM, Steinberg S, Sealock J, Karlsson IK, Hagg S, Athanasiu L, et al. Genome-wide meta-analysis identifies new loci and functional pathways influencing Alzheimer's disease risk. Nat Genet. 2019;51:404–13.
68. Kamboh MI, Demirci FY, Wang X, Minster RL, Carrasquillo MM, Pankratz VS, Younkin SG, Saykin AJ, Alzheimer's Disease Neuroimaging I, Jun G, et al. Genome-wide association study of Alzheimer's disease. Transl Psychiatry. 2012;2: e117.
69. Li YQ, Tan MS, Wang HF, Tan CC, Zhang W, Zheng ZJ, Kong LL, Wang ZX, Tan L, Jiang T, et al. Common variant in PTK2B is associated with late-onset Alzheimer's disease: a replication study and meta-analyses. Neurosci Lett. 2016;621:83–7.
70. Haas LT, Strittmatter SM. Oligomers of amyloid beta prevent physiological activation of the cellular prion protein-metabotropic glutamate receptor 5 complex by glutamate in Alzheimer disease. J Biol Chem. 2016;291:17112–21.
71. Kaufman AC, Salazar SV, Haas LT, Yang J, Kostylev MA, Jeng AT, Robinson SA, Gunther EC, van Dyck CH, Nygaard HB, Strittmatter SM. Fyn inhibition rescues established memory and synapse loss in Alzheimer mice. Ann Neurol. 2015;77:953–71.
72. Brody AH, Strittmatter SM. Synaptotoxic signaling by amyloid beta oligomers in Alzheimer's disease through prion protein and mGluR5. Adv Pharmacol. 2018;82:293–323.
73. Brody AH, Nies SH, Guan F, Smith LM, Mukherjee B, Salazar SA, Lee S, Lam TKT, Strittmatter SM. Alzheimer risk gene product Pyk2 suppresses tau phosphorylation and phenotypic effects of tauopathy. Mol Neurodegener. 2022;17:32.
74. Lee S, Salazar SV, Cox TO, Strittmatter SM. Pyk2 Signaling through Graf1 and RhoA GTPase is required for amyloid-beta oligomer-triggered synapse loss. J Neurosci. 2019;39:1910–29.
75. Dickson DW. Multinucleated giant cells in acquired immunodeficiency syndrome encephalopathy. Origin from endogenous microglia? Arch Pathol Lab Med. 1986;110:967–8.
76. Michaels J, Price RW, Rosenblum MK. Microglia in the giant cell encephalitis of acquired immune deficiency syndrome: proliferation, infection and fusion. Acta Neuropathol. 1988;76:373–9.
77. Kreutzberg GW. Microglia: a sensor for pathological events in the CNS. Trends Neurosci. 1996;19:312–8.
78. Hornik TC, Neniskyte U, Brown GC. Inflammation induces multinucleation of microglia via PKC inhibition of cytokinesis, generating highly phagocytic multinucleated giant cells. J Neurochem. 2014;128:650–61.
79. Peterson PK, Gekker G, Hu S, Anderson WB, Teichert M, Chao CC, Molitor TW. Multinucleated giant cell formation of swine microglia induced by Mycobacterium bovis. J Infect Dis. 1996;173:1194–201.
80. Ahmadzadeh K, Vanoppen M, Rose CD, Matthys P, Wouters CH. Multinucleated giant cells: current insights in phenotype, biological activities, and mechanism of formation. Front Cell Dev Biol. 2022;10:873226.
81. Valimaki E, Miettinen JJ, Lietzen N, Matikainen S, Nyman TA. Monosodium urate activates Src/Pyk2/PI3 kinase and cathepsin dependent unconventional protein secretion from human primary macrophages. Mol Cell Proteomics. 2013;12:749–63.
82. Combs CK, Johnson DE, Cannady SB, Lehman TM, Landreth GE. Identification of microglial signal transduction pathways mediating a neurotoxic response to amyloidogenic fragments of beta-amyloid and prion proteins. J Neurosci. 1999;19:928–39.
83. Belrose JC, Jackson MF. TRPM2: a candidate therapeutic target for treating neurological diseases. Acta Pharmacol Sin. 2018;39:722–32.
84. Yamamoto S, Shimizu S, Kiyonaka S, Takahashi N, Wajima T, Hara Y, Negoro T, Hiroi T, Kiuchi Y, Okada T, et al. TRPM2-mediated Ca2+influx induces chemokine production in monocytes that aggravates inflammatory neutrophil infiltration. Nat Med. 2008;14:738–47.
85. Alawieyah Syed Mortadza S, Sim JA, Neubrand VE, Jiang LH. A critical role of TRPM2 channel in Abeta(42) -induced microglial activation and generation of tumor necrosis factor-alpha. Glia. 2018;66:562–75.
86. Ryzhakov G, Almuttaqi H, Corbin AL, Berthold DL, Khoyratty T, Eames HL, Bullers S, Pearson C, Ai Z, Zec K, et al. Defactinib inhibits PYK2 phosphorylation of IRF5 and reduces intestinal inflammation. Nat Commun. 2021;12:6702.
87. Corsi JM, Rouer E, Girault JA, Enslen H. Organization and post-transcriptional processing of focal adhesion kinase gene. BMC Genomics. 2006;7:198.
88. Hall JE, Fu W, Schaller MD. Focal adhesion kinase: exploring Fak structure to gain insight into function. Int Rev Cell Mol Biol. 2011;288:185–225.
89. Schaller MD. Cellular functions of FAK kinases: insight into molecular mechanisms and novel functions. J Cell Sci. 2010;123:1007–13.
90. Wu Y, Li N, Ye C, Jiang X, Luo H, Zhang B, Zhang Y, Zhang Q. Focal adhesion kinase inhibitors, a heavy punch to cancer. Discov Oncol. 2021;12:52.
91. Jeon M, Hong S, Cho H, Park H, Lee SM, Ahn S. Targeting FAK/PYK2 with SJP1602 for anti-tumor activity in triple-negative breast cancer. Curr Issues Mol Biol. 2023;45:7058–74.
92. Saito T, Matsuba Y, Mihira N, Takano J, Nilsson P, Itohara S, Iwata N, Saido TC. Single app knock-in mouse models of Alzheimer's disease. Nat Neurosci. 2014;17:661–3.

93. Sato K, Watamura N, Fujioka R, Mihira N, Sekiguchi M, Nagata K, Ohshima T, Saito T, Saido TC, Sasaguri H. A third-generation mouse model of Alzheimer's disease shows early and increased cored plaque pathology composed of wild-type human amyloid beta peptide. J Biol Chem. 2021;297:101004.
94. Giralt A, de Pins B, Cifuentes-Diaz C, Lopez-Molina L, Farah AT, Tible M, Deramecourt V, Arold ST, Gines S, Hugon J, Girault JA. PTK2B/Pyk2 overexpression improves a mouse model of Alzheimer's disease. Exp Neurol. 2018;307:62–73.
95. Kilinc D, Vreulx AC, Mendes T, Flaig A, Marques-Coelho D, Verschoore M, Demiautte F, Amouyel P, Neuro CEBBB, Eysert F, et al. Pyk2 overexpression in postsynaptic neurons blocks amyloid beta(1–42)-induced synaptotoxicity in microfluidic co-cultures. Brain Commun. 2020;2:fcaa139.

Publisher's Note